Chemical Science

ROYAL SOCIETY OF CHEMISTRY

REVIEW

View Article Online
View Journal | View Issue

Cite this: *Chem. Sci.*, 2025, **16**, 19072

Microenvironment modulation of single-atom sites and its applications in Fenton-like reactions

Na Wang, * Jie Yang, Sixun Li, Ziqiu Ren * and Qun Xu *

Single-atom catalysts (SACs) featuring ultrahigh atom utilization, tunable coordination environments, and distinct structure–activity relationships have emerged as a prominent class of catalysts in heterogeneous Fenton-like reactions. Precise modulation of microenvironments around active single-atom sites offers a promising avenue to enhance catalytic activity, direct reaction pathways, and elucidate underlying mechanisms; however, achieving such control remains a significant challenge. This review systematically delineates the microenvironment modulation strategies of SACs in heterogeneous Fenton-like systems, encompassing coordination environment engineering, support/ligand-mediated electronic regulation, spatial confinement regulation, and external field effects. By manipulating ligand properties, modifying supports, altering electronic structures, controlling the local environment and introducing an external field, these strategies synergistically enhance the catalytic performance and regulate the underlying reaction mechanisms. Moreover, analysis of correlations among active-center microenvironment structures, Fenton reactivity, and reactive oxygen species (ROS) generation pathways offers valuable insights for future research and development in this domain. Finally, by addressing the critical challenges in SAC design and nascent microenvironment engineering, this review delineates future research directions for SACs in Fenton-like systems and analogous catalytic processes.

Received 14th July 2025
Accepted 23rd September 2025

DOI: 10.1039/d5sc05230k

rsc.li/chemical-science

1. Introduction

Water contamination by organic contaminants has emerged as a key obstacle to global sustainable development. Originating from diverse sources including industrial effluents, agricultural pesticides, and municipal waste, these contaminants are toxic, recalcitrant, and bioaccumulative, posing severe threats to ecological balance and human health.[1] Advanced oxidation processes (AOPs) using peroxymonosulfate (PMS) as an oxidant have been widely investigated as a highly efficient water treatment technology due to their intrinsic advantages such as high efficiency, simple operation, cost-effectiveness, and environmental benignity.[2–4] At present, the mainstream mechanism governing the decomposition of pollutants in PMS–AOP systems is radical oxidation, which encompasses the sulfate radical ($SO_4^{\bullet-}$),[5] hydroxyl radical ($HO^{\bullet}$),[6] and superoxide radical ($O_2^{\bullet-}$).[7] In addition, non-radical oxidation involving singlet oxygen ($^1O_2$), surface-bound active species, high-valence metal–oxo species (M(IV)=O) and an electron transfer process (ETP)

Henan Institute of Advanced Technology, Zhengzhou University, Henan, 450002, P. R. China. E-mail: nawang@zzu.edu.cn

Na Wang

Na Wang is currently an assistant professor at Henan Institute of Advanced Technology, Zhengzhou University. She received her Ph.D. degree in Chemical Engineering and Technology in 2020 at Harbin Institute of Technology. She is mainly engaged in the design and synthesis of nanocatalytic materials and their research in water pollution remediation.

Jie Yang

Jie Yang graduated from Huazhong Agricultural University with a B.Sc. degree in Chemistry in 2024. She is currently pursuing her M.Sc. degree at Zhengzhou University. Her scientific interest focuses on nanocatalytic materials for water pollution remediation.

with milder oxidation capability and high selectivity has been increasingly recognized as a predominant mechanism for the elimination of contaminants in water.[8–12] The formation of different reaction pathways is closely related to the properties and surface structures of catalysts. Transition metals can activate PMS *via* surface interactions between active metal sites and PMS molecules. The low bond energy (33.5 kcal mol^{-1}) and extended O–O bond length (1.497 Å) of PMS inherently facilitate electron acceptance from metal centers, leading to O–O bond cleavage and radical generation.[13–15] However, severe metal leaching and suboptimal catalytic performance remain the overriding bottlenecks for the development of metal-based catalysts. Carbonaceous materials are emerging heterogeneous PMS activators due to their metal-free and earth-abundant properties, huge specific surface area, and tunable electronic features.[16–18] Carbon-based catalysts mitigate metal ion-induced secondary pollution, with heteroatom doping and surface functionalization strategies boosting catalytic activity. Nevertheless, the intrinsic inertness and intricate surface architecture of carbon materials impose constraints on their catalytic activity enhancement, while the ambiguous reaction mechanisms hinder rational catalyst design and practical applications.

Single-atom catalysts (SACs), integrating the advantages of metal-based and carbon-based catalysts, have attracted increasing attention in Fenton-like reactions owing to their ultrahigh atomic utilization, flexible coordination structure, and distinct structure–activity relationship.[19–21] Compared with traditional catalysts, their high atomic utilization and robust metal–N components strengthen the metal–support interactions and effectively mitigate the long-standing metal leaching issue. In addition, SACs possess well-defined isolated active sites, which allow precise identification of catalytic sites and thereby facilitate the exploration of catalytic essence and reaction pathways. Moreover, SACs inherit the merits of carbon-based materials such as tunable electronic properties of the support, while overcoming their intrinsic inertness through the introduction of active metal sites, thus achieving enhanced catalytic performance. Based on previous reports, the activity and reaction mechanisms of SACs are closely associated with the microenvironment surrounding their active centers.[22–24] The local microenvironment exerts a profound influence on the electronic properties of active sites, the adsorption and activation of reactants, and the subsequent reaction pathways. For instance, the coordination ligands surrounding a single-atom center can fine-tune its electron density and thereby affect the capacity to activate oxidants.[25,26] Due to the robust interaction between metal centers and supports, the inherent electronic and geometric characteristics of atomic active sites are highly contingent upon their surrounding microenvironment.[27–29] Additionally, the nanoconfined environment can enhance the interaction between active centers and PMS/PDS and lower the activation energy barriers, thus guiding the reaction path and improving the selectivity of the generated active species.[30,31] Therefore, accurate manipulation of the local geometric and electronic environment around the single atomic sites provides a highly viable strategy, which is capable of governing the catalytic activity and selectivity of catalytic reactions, curtailing the formation of undesired by-products, and allowing for in-depth investigations into reaction mechanisms at the molecular scale.

So far, a large number of studies have explored many aspects of microenvironment modulation and consequent changes in catalyst activity and reaction mechanisms in Fenton-like systems.[32,33] However, the intricate interplay between catalyst surface structures, diverse chemical properties, and their dynamic nature has obscured the fundamental relationships between microenvironment modulation strategies, electronic structure transformations, and reaction mechanism evolution. For instance, although some studies have shown that introducing axial ligands into the metal–N_4 active center of SACs can enhance their Fenton activity, the potential mechanisms underlying the types and properties of ligands and axial coordination patterns in controlling this enhancement have not

Ziqiu Ren

Ziqiu Ren received his Ph.D. degree from the School of Chemistry and Chemical Engineering at Harbin Institute of Technology in 2020. He then joined Henan Institute of Advanced Technology, Zhengzhou University. His research interests include multifunctional organic–inorganic hybrid materials, nano-optoelectronic devices, and perovskite solar cells. He is also interested in the synthesis of nanocatalytic materials and their application in water pollution remediation.

Qun Xu

Qun Xu is a full professor at Henan Institute of Advanced Technology, College of Materials Science and Engineering, Zhengzhou University. She obtained her PhD in Physical Chemistry from Institute of Chemistry, Chinese Academy of Science in 1999. And in 2001, she finished her postdoctoral work at Karlsruhe Nuclear Center in Germany and returned back to China. In recent years, she has focused on the design, synthesis and performance exploration of novel nanostructures with the assistance of supercritical CO_2 for green energy conversion and water treatment.

been fully understood.[34,35] Additionally, the impact of the substrate material on the microenvironment and its subsequent effect on the reaction has not been thoroughly investigated. There is also a scarcity of studies considering the combined effects of multiple microenvironmental factors on both catalyst activity and reaction pathways. Consequently, a critical knowledge gap persists: there remains a paucity of systematic, comprehensive reviews that synthesize these fragmented insights, systematically dissect these multifaceted interactions and provide a clear roadmap for rationally engineering the microenvironment of SACs to optimize Fenton-like performance for water treatment.

In view of these research gaps, this review comprehensively and deeply discusses the applications of microenvironment regulation strategies for SACs in enhancing the performance of Fenton-like reactions and elucidating the reaction mechanism (Scheme 1). These strategies encompass: (1) coordination environment modulation, where the nature and number of ligands around active centers are manipulated; (2) support-effect regulation, involving support modification and interactions between active sites and supports; (3) external field modulation, involving the electronic structure optimization of active sites and regulation of the generation of ROS and reaction rates; (4) spatial confinement regulation, such as modulating molecular orientation and reaction dynamics. Subsequently, we highlight the remarkable breakthroughs enabled by microenvironment regulation of active centers in carbon-based SACs, including enhanced Fenton-like activity, elucidation of reaction mechanisms, and improved selectivity. The relationships between the microenvironment structures of diverse active centers and Fenton activity, as well as reaction mechanisms, are analyzed, providing a reference for precise engineering of active-center microstructures in SACs. Finally, we discuss the challenges faced and provide perspectives to guide the rational design of SACs for future catalysis applications.

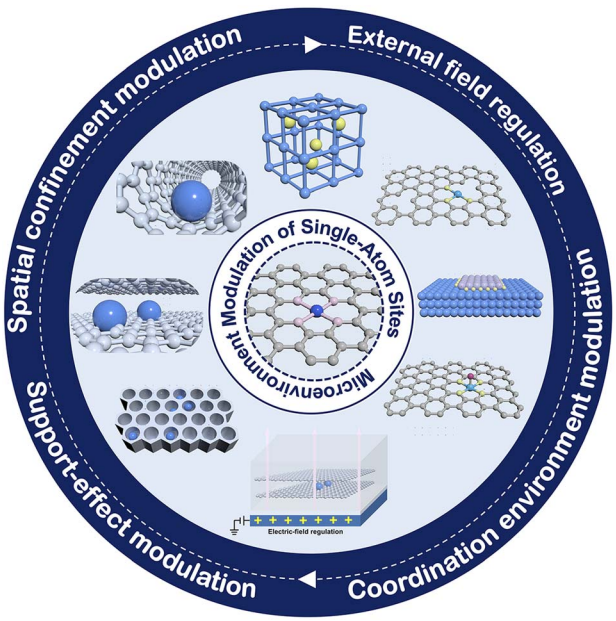

Scheme 1 Overview of the main topics of this review: microenvironment modulation strategies for single-atom sites.

2. Microenvironment and electronic structure characteristics of single atom catalysts

2.1 Compositions and intrinsic advantages

Single-atom catalysts (SACs) are a special type of supported catalyst, mainly composed of active single atoms and supports. The active metal components exist in the form of isolated single atoms on the surface of the support, rather than forming nanoparticles or clusters. The active single atoms are usually transition metal atoms, such as Fe, Co, Ni, Mn, Pt, Pd, Au, *etc.*,[36,37] which have abundant d-electron orbitals and exhibit unique catalytic ability through interactions with ligands and supports. The role of the support is to provide a high specific surface area for single atom dispersion and stabilization. Typical support materials encompass metal oxides (TiO_2, CeO_2, Fe_2O_3, *etc.*),[38–41] carbon materials (activated carbon, carbon nanotubes, graphene, *etc.*), metal–organic frameworks (MOFs), *etc.*[42–44] SACs have emerged as an innovative strategy to address the bottlenecks of traditional heterogeneous catalysts in Fenton-like reactions, such as low atomic utilization rate, uneven active sites, and trade-off between catalytic activity and stability, demonstrating distinct advantages. Firstly, the highly dispersed single-atom sites on the support achieve nearly 100% atomic utilization, effectively overcoming the inefficiency caused by atomic aggregation and reducing catalyst costs. Secondly, SACs exhibit unique electronic structures with coordination environments that can be precisely modulated by manipulating support types and ligand atoms, thereby altering the electron density of single atoms and enhancing reactant activation. For example, the typical metal–N_4 structure (M–N–C) in SAC on carbon supports has been widely demonstrated to be active in significantly promoting PMS or PDS activation in Fenton-like reactions.[45,46] Finally, the well-defined active sites of SACs facilitate the in-depth investigation of catalytic mechanisms. Through the integration of advanced characterization techniques and density functional theory (DFT) calculations, the structure of active sites and reaction pathways can be elucidated, providing a robust theoretical foundation for rational catalyst design.[36] These features endow SACs with remarkable potential in Fenton-like reactions, offering new avenues for environmental remediation.

2.2 Supports and ligands

The main function of supports is to provide a platform with high specific surface area for metal atoms to disperse in an isolated state, and to prevent metal agglomeration through interaction with metal single atoms. Ligands provide a stable coordination environment for single atoms by forming coordination or chemical bonds with them, preventing their migration and agglomeration during reaction processes. Electronic interactions between the supports, ligands, and single-atom active centers are pivotal for elucidating the performance of

SACs and the underlying reaction mechanism. For example, the strong metal–support interaction (SMSI) can not only enhance the stability of metal atoms on support surfaces, inhibiting single-atom migration and agglomeration under intricate reaction conditions, but also modify the electronic structures of metal atoms.[47–49] It may also influence the electronic properties of supports, generating a synergistic effect to boost catalytic activity and selectivity. Specifically, the carbonaceous supports modulate the electron density of single atoms *via* a charge transfer mechanism. The presence of defects within the carbon frameworks or the incorporation of dopant elements significantly augments the charge transfer phenomenon. These structural alterations enable more pronounced electronic interactions between the support and single atoms, thereby exerting a stronger influence on the electronic properties of active sites.[50] For example, Wu *et al.* introduced abundant topological defects into the carbon matrix hosting Fe–N_4 sites. Synergistic interactions between Fe–N_4 units and neighboring defects optimize the electronic structure of the d-band center of Fe *via* long-range interactions, thereby enhancing the intrinsic activity of Fe–N_4 sites.[51] In addition, the electron-donating or electron-accepting ability of ligands also affects the electronic structure of single atoms. Several outstanding reviews have comprehensively summarized strategies for the regulation of electronic structure of SACs and highlighted their promising applications with remarkable performance.[52–55] These reviews collectively indicate that electronegativity differences of coordination atoms (N, O, S) can alter the distribution of electrons in the d-band of the metal centers *via* charge transfer. Strong electronegative ligands reduce metal electron density, while weak ones enhance metal–support interactions through electron donation. Meanwhile, ligands can also have weak interactions with reactants, constructing a synergistic catalytic network.[56] By regulating the reaction pathways through electronic and spatial effects, they can achieve multi-dimensional control over the adsorption and activation of reactants, reaction selectivity, and catalytic stability, significantly enhancing the performance of SACs.

2.3 Electron delocalization and charge distribution

The interaction between a single-atom active center and its surrounding environment (supports and ligands) can induce an electron delocalization phenomenon, which breaks the traditional local electron distribution pattern, enabling a single atom to form a coordinated electron system with the surroundings. Xin *et al.* reported Zn-based SACs with coexisting Zn–N_4 and Zn–N_3 configurations for PDS activation.[57] The low-coordinated Zn–N_3 induces the electron delocalization phenomenon, generating rich delocalized electrons that lower the oxidation state of the Zn atom and thereby facilitate electron transport between Zn–N_x sites and PDS. Electron delocalization not only alters the electron distribution of a single atom, but also affects its compatibility with the molecular orbitals of reactants, thereby regulating the adsorption and activation processes of reactants. Appropriate electron delocalization can optimize the adsorption strength of PMS/PDS molecules on single atoms, avoiding the difficulty in converting oxidants due to excessive adsorption or the desorption of reactants due to insufficient adsorption. As is well known, the selective generation of high-valent metal–oxo species in PMS AOP systems poses a significant challenge due to relatively high occupancy of the 3d orbitals in metals and high bond dissociation energy associated with metal deprotonation processes. Liu *et al.* employed the O doping strategy to break the balance of the Co–N_4 moiety to construct an asymmetric CoN_3O, inducing the targeted production of Co^{IV}=O.[58] Computational studies demonstrated that the non-symmetric coordination of CoN_3O triggers extensive electron delocalization around the Co centers, which not only enhances the adsorption of peracetic acid and promotes the cleavage of its peroxy O–O bond, but also gives rise to an auxiliary local electric field due to the unique electronic asymmetry. This field enabled the cleavage of the O–H bond through a proton-coupled electron transfer process, ultimately driving the formation of CoN_3O species.

In some systems with conjugated structures, such as nitrogen-containing heterocycles (pyridine, porphyrin), carbon-based conjugated networks (graphene, graphitic carbon nitride), *etc.*, the electrons of single atoms will participate in the electron delocalization network of the entire system, causing the charges to be distributed over a larger range.[59,60] The charge distribution of SACs is closely correlated with the activity and selectivity of the Fenton-like reactions. The charge density variation of the central atom affects its REDOX ability towards the oxidant molecules. The efficient electron acceptance or donation facilitates the charge transfer process during the reaction and modifies the formation energy barrier of intermediates and the generation pathways of ROS, thereby significantly enhancing the overall efficiency of the catalytic reaction.

2.4 Diversity of oxidation states and valence states

In general, the oxidation states and valence states of single metal sites in SACs are diverse and may undergo dynamic changes during the catalytic reaction. Such changes are closely related to the reaction conditions, the characteristics of the reactants, and the interactions between metal sites and their local environments.[61–64] For instance, tailoring the electronic structure of SACs can induce valence-state changes of metal sites, optimize reaction pathways, and thus enhance catalyst activity. As reported by Cui *et al.*,[65] modulating the electronic configuration of polymeric carbon nitride (CN), that is, increasing the C/N ratio, induces a positive shift in the valence states of these Fe sites, subsequently lowering the energy barriers for Fe^{IV}=O formation and enhancing PMS activation efficiency. In addition, the unique electronic structure of a single atomic site significantly enhances its capacity for electron gain or loss, enabling it to shift among different oxidation states and consequently lower the energy barrier involved in the formation of reaction intermediates. In Song's work,[63] the unsaturated Co sites in CoN_3 with a high-spin state exhibit a superior electron-donating capacity and facilitate significant electron transfer, thereby promoting the valence transition from Co(II) to Co(IV). In contrast, the saturated Co

sites in CoN_4 with a low-spin state merely induce the conversion from Co(II) to Co(III), leading to the generation of radicals. Apparently, the dynamic modulation of oxidation states acts as the pivotal driving force for catalysis, facilitating the adsorption, activation, transformation, and desorption of PMS and substrate molecules on the catalyst surface. The electronic structure of metal sites, which directly governs their oxidation state stability and redox activity, is fundamentally shaped by their coordination environment. For instance, electronegative ligands (N, O) withdraw electrons from metal centers, promoting higher oxidation states. Compared with the saturated coordination configuration, a lower coordination number can reduce ligand field splitting, stabilize the high-spin state, and thereby facilitate oxidation state transition. Overall, these electronic structure characteristics of SACs are dynamically shaped by the local microenvironment of single-atom centers. They are interrelated and influence each other, jointly determining the catalytic performance of SACs. They also provide a theoretical basis for optimizing the performance of SACs through the rational design and regulation of their electronic structures. Rational microenvironment regulation through coordination engineering, support modification, or spatial confinement allows precise tuning of electronic structure, guiding the design of high-performance Fenton-like catalysts (Fig. 1).

3. Microenvironment modulation of SACs in Fenton-like systems

3.1 Coordination environment modulation

The coordination environment of SACs, for example, the types, numbers, and spatial arrangements of coordinating atoms around the single-atom sites, significantly affect the electronic structure, thus governing the catalytic activity, selectivity and stability of SACs. Taking the metal–nitrogen (M–N) coordination structure as an example, nitrogen atoms can attract electrons of the metal centers, reduce the electron cloud density of the metal atoms and change the electron distribution in the d orbitals when they coordinate with single metal atoms, because nitrogen atoms have a relatively high electronegativity. Therefore, the adsorption and activation abilities of the metal atoms towards reactant molecules can be precisely modulated. For instance, in an Fe–N–C single-atom catalyst, the $Fe–N_4$ coordination changes the position of the d-band center of the Fe atom, optimizing the adsorption energy for PMS molecules and thus enhancing the activity for PMS activation.[66] Heteroatom introduction modifies metal atom coordination environments, enhances electronic delocalization around metal atoms, and disrupts the symmetric electronic distribution of metal atoms in $M–N_4–C$ SACs.[67] Moreover, different coordinating atom combinations yield diverse electronic effects. Oxygen coordination usually renders metal atoms more positively charged, whereas sulfur coordination generally increases the electron density of the metal atom.[68,69] Given the significant influence of coordination environments on SACs, regulating their coordination environment for Fenton-like reactions is a key research direction, which will be discussed in the following sections.

3.1.1 Ligand species and structure. The types and structures of ligands in SACs profoundly impact the electronic state, coordination environment, catalytic activity, and reaction mechanism of SACs. Comprehending the impact of ligand regulation on the Fenton-like activity of SACs is essential for the development of high-performance Fenton-like catalytic systems. Among these, nitrogen-containing ligands are most prevalent. The application of Co SACs with a typical $Co–N_4$ configuration in a PMS-based system was reported for the first time by Zhang's group in 2018.[44] The $Co–N_4$ was identified as the dominant active site for PMS conversion, while the adjacent

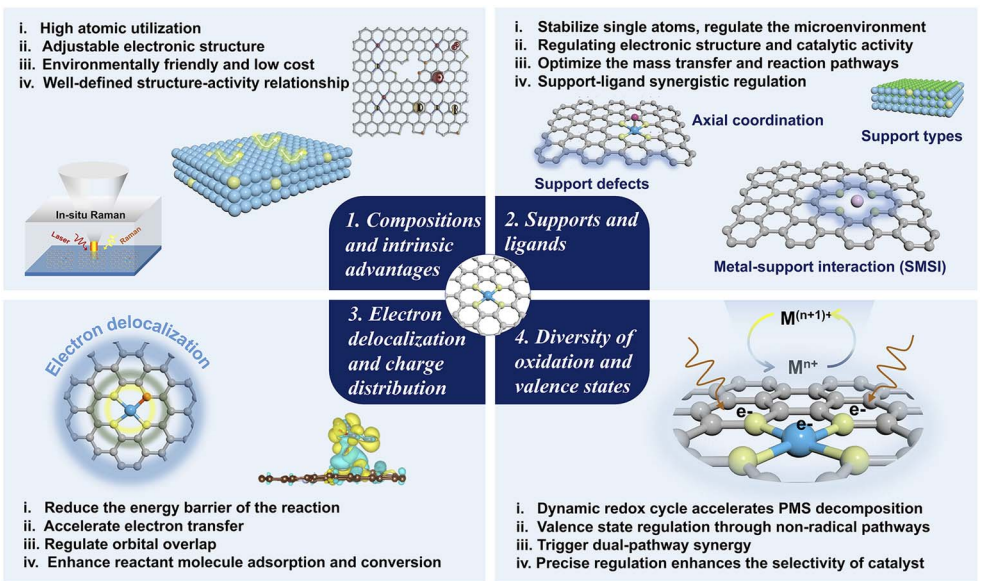

Fig. 1 Structural and microenvironmental characteristics of single atom catalysts.

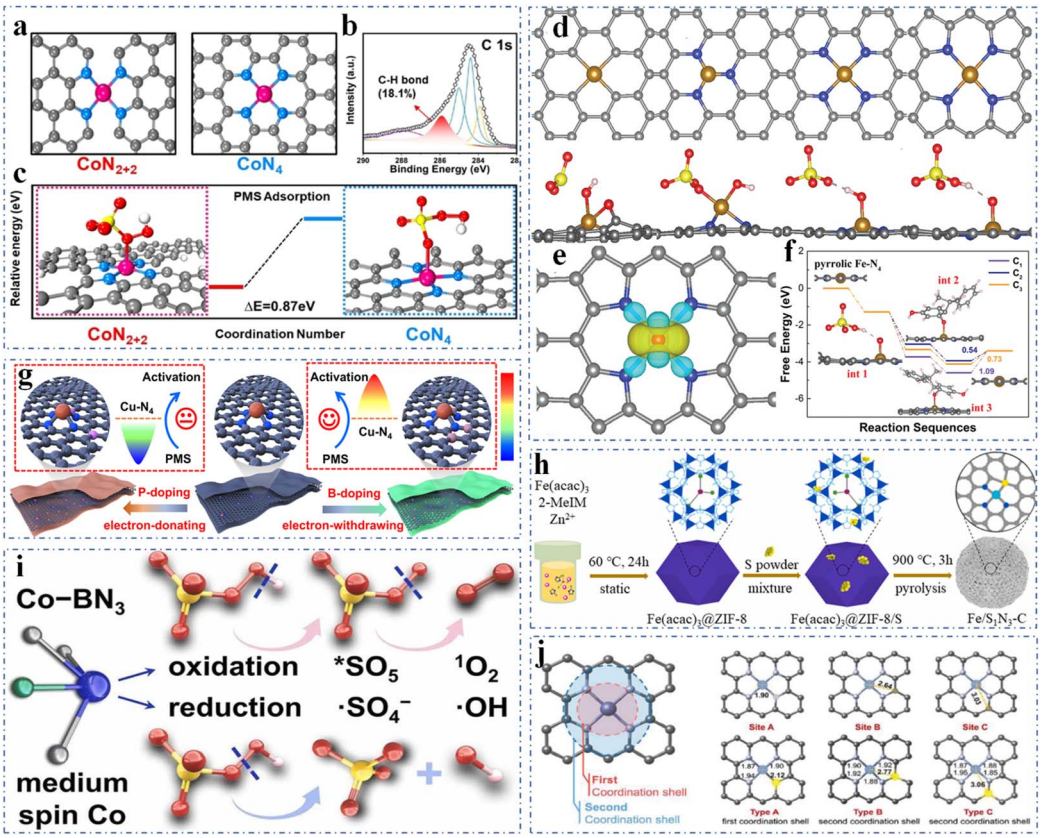

Fig. 2 (a) Atomic structure of the CoN_{2+2} and CoN_4 active sites of Co-SA. (b) XPS spectrum of C of Co-SA. (c) Calculated free energy evolution of PMS adsorption on CoN_{2+2} and CoN_4 sites. Copyright 2020, Wiley-VCH. (d) Optimized models of SA-Fe/CN and corresponding optimized structures for PMS activation: from left to right are FeC_4, FeN_3, pyridinic FeN_4, and pyrrolic FeN_4, respectively. (e) Charge density difference of the pyrrolic FeN_4 model with Fe–oxo species. (f) Energy profile of the oxidation of BPA on pyrrolic FeN_4 through three possible pathways. Copyright 2022, Wiley-VCH. (g) The preparation strategy for Cu–N_4/C–B and Cu–N_4/C–P. Copyright 2022, PANS. (h) The synthesis of Fe–SN–C. Copyright 2024, Elsevier. (i) Co-SAC coordination microenvironment regulation and corresponding ROS transformation. Copyright 2024, American Chemical Society. (j) Schematic diagram of coordination shell and distances from the atoms to Fe centers. Copyright 2025, Wiley-Advanced.

pyrrolic N site functioned as an adsorption site for organic pollutants. This configuration shortened the migration distance of active species (*i.e.*, $^1O_2$) and thus promoted contaminant degradation. Additionally, other single-atom Fe and Mn SACs have also been employed for PMS activation, in which the Mn–N_4 configuration facilitated the decomposition of PMS into active radicals ($SO_4^{\bullet-}$ and $HO^{\bullet}$),[70] whereas the Fe–N_4 moiety predominantly generated $^1O_2$,[71] high-valence Fe–oxo species[72,73] or induced an electron transfer process.[74] Some advanced reviews have comprehensively summarized and delved deeply into the influence mechanism of the metal active centers in SACs on their catalytic performance.[54,55,75] The distinct electronic structures of metal centers and their varied interactions with PMS endow different SACs with diverse PMS activation abilities and reaction regimes. For instance, Fe-SAC and Cu-SAC with identical coordination structures (Cu–N_4 and Fe–N_4) show distinct PMS activation activities and trigger different ROS generation mechanisms,[76] which mainly arises from the differences in the spin states of different metal atoms. To enhance the reaction kinetics of PMS activation, multiple approaches have been devised to boost the intrinsic activity of single-atom sites. For example, in Mi's work, manipulating the structures of the single metal sites revealed that PMS adsorbs and activates more efficiently on the CoN_{2+2} site than on the CoN_4 site (Fig. 2a–c).[77]

Different nitrogen coordination forms, including pyridinic nitrogen, pyrrolic nitrogen, and graphitic nitrogen, distinctly modulate the electronic structures and Fenton-like activities of SACs. Xiong *et al.* pointed out the discrepant role of different N species on an SA-Fe/CN catalyst in the PMS activation reaction (Fig. 2d–f).[78] The target molecule was preferentially adsorbed onto graphitic N. Pyrrolic N coordinated with Fe(III) was the key determinant in driving the reaction forward because the d-band center of the pyrrolic-type Fe–N_4 sites was positioned at a lower energy level, giving rise to antibonding states that possessed lower energy levels and higher electron occupancy. This energetic configuration facilitated the formation of Fe–oxo species on the active sites, improving PMS activation kinetics. Although pyridinic N coordinated with Fe(II), its contribution to the reactivity of SA-Fe/CN was relatively small. In contrast, Zhang *et al.* demonstrated that the adsorption of PMS on Co in pyridine-type Co–N_4 was stronger than that on Co in pyrrole-

type Co–N_4 because pyridinic N had a remarkable ability to reshape and fine-tune the electron configuration of the Co 3d orbital.[79] Such orbital modification led to a significant shift of the d-band center towards the Fermi level, triggering the generation of low spin-state Co species, thus promoting more efficient electron transfer and decreasing the activation energy required for PMS activation.

Previous studies have determined that PMS adsorption strength at the M–N_4 site controls its activation by SACs. However, recent findings show that strong PMS–metal binding may cause deactivation of the M–N_4 site. To overcome this, alien heteroatoms such as sulfur (S),[80,81] phosphorus (P), boron (B),[82,83] and oxygen (O)[58,84–86] are incorporated into the carbon matrix adjacent to the M–N_4 moiety to create an asymmetric coordination structure to regulate the electronic structure of M–N_4 and increase the electron transfer ability of SACs. According to Zhou's findings, the electronic configuration of Cu–N_4 sites in Cu SACs could be precisely tuned by embedding specific heteroatoms (B/P) within N-doped carbon supports (Fig. 2g).[87] Owing to the electronegativity disparity between P and B, the electron-deficient Cu–N_4/C–B exhibited the highest oxidation activity among various Cu–N_4 SACs in Fenton-like reactions. The long-range interaction with B atoms reduced the electron density of Cu active sites, shifted the d-band center downward, and optimized the PMS activation adsorption energy. In contrast, Cu–N_4/C–P showed a notable decrease in performance. In contrast to the symmetric Co–N_4 structure, Yang *et al.* found that the incorporation of P or S atoms disrupted the local symmetry, thereby generating an asymmetric electric field in the vicinity of the Co center. This field enabled the formation of $Co^{(IV)}$=O from PMS through a coupled electron-proton transfer.[88] Dai *et al.* constructed an Fe–SN–C catalyst by incorporating an S atom into the first coordination shell of the Fe single-atom site (Fe–S_1N_3) (Fig. 2h).[89] Introduction of S atoms reduced the loss of valence electrons of Fe atoms, keeping Fe in a lower oxidation state and making it easier to provide electrons to activate PMS. Meanwhile, the S/N double coordination increased the electron density of Fe atoms, brought the d-band center closer to the Fermi level, optimized the activation energy of PMS decomposition, and enhanced the interaction between Fe and PMS molecules. In addition, S coordination increased the number of unpaired d electrons of Fe atoms, enhanced the hybridization of Fe 3d and O 2p orbitals in PMS, and promoted the rapid generation of Fe(IV)=O. Fan *et al.* employed the coordination engineering strategy of SAC and used Fe–O_4/C, FeN_2O_2/C, and Fe–N_4/C as model catalysts to further explain the Sabatier principle in Fenton-like reactions.[84] They pointed out that FeN_2O_2/C with a moderate d-band center and appropriate PMS adsorption energy exhibited a lower rate-determining step barrier for $^1O_2$ generation. However, the introduction of foreign heteroatoms does not invariably lead to enhanced catalyst activity. Lai's group combined theoretical calculations and experimental results to prove that replacing N with C and coordinating with an Fe atom (from Fe–N_4 to Fe–N_3C_1 and Fe–N_2C_2) reduced the catalytic activity of the Fe–N_xC_{4-x} sites in PMS activation.[90] This substitution caused the Fe d-band center to move more negatively relative to the Fermi level. As a result, the weakened PMS adsorption led to a significant reduction in the kinetics of $^1O_2$ generation, inhibiting the Fenton-like activity of the catalyst. Additionally, asymmetric coordination construction exerts an influence on the spin state, and this influence extends to the valence electron distribution in the extra-atomic-site d-orbitals, ultimately leading to changes in the reaction energy. Sun *et al.* elucidated the effects of asymmetric Co–BN_3 structure on the spin state of Co (Fig. 2i).[82] Their findings showed that the spin state of Co underwent a change from a high-spin to a medium-spin state after B doping, which improved the electron absorption and donation capabilities of the d-orbitals of Co SAC. As a result, the energy barrier for redox reactions in PMS was lowered, facilitating the generation of sulfate radicals and singlet oxygen. Despite the widespread acknowledgment that heteroatom doping can effectively tune the electronic structure of active sites, reduce the reaction energy barrier, and optimize the reaction pathway, the precise location of heteroatom doping, for example, in the first shell, the second shell, or randomly dispersed within the carbon network, remains ambiguous. Elucidating the impact of heteroatoms in different coordination shells on the electronic structure and catalytic activity of the active center is of critical significance. Zhang *et al.* demonstrated that S in the second coordination shell more efficiently optimized the adsorption–desorption energy barriers of oxygen-containing intermediates at active sites, thus exhibiting prominent performance in zinc–air batteries (Fig. 2j).[91] Furthermore, Zou *et al.* discovered that the Fe SAC with S in the second shell (Fe-NSC-L) could activate PMS to selectivity generate nearly 100% Fe^{IV}=O and showed optimal organic oxidation ability as compared to the catalyst with S in the first shell.[92] Theoretical calculations indicated that second-shell S mildly tuned the electronic properties of Fe active sites, increasing Fe–O antibonding orbital occupancy in Fe–PMS*. This promotes O–O bond breakage and selective Fe^{IV}=O formation for enhanced catalysis.

Overall, significant progress has been made in the regulation of ligand types and coordination structures of SACs in Fenton-like systems, but many challenges still remain. For example, the stability of coordination structures in highly oxidizing environments remains a critical challenge. Future work should focus on designing robust coordination environments, such as leveraging supports with strong binding affinities or introducing protective ligands, to enhance catalyst durability. In addition, precise regulation of ROS and reaction pathways in single-atom catalysis represents another critical frontier. Future research should focus on developing strategies to regulate the generation of reactive oxygen species and their selectivity such as: (1) applying nanoconfinement effects to switch the mechanism from $^1O_2$ to ETP pathways, thereby enhancing degradation efficiency for electron-rich pollutants; (2) engineering dual-atom sites to synergistically tune ROS distribution ratios through cooperative metal–metal interactions. Such advancements will enable more targeted and efficient environmental remediation while minimizing undesired side reactions.

3.1.2 Coordination number. The modulation of ligand numbers in SACs exerts a profound impact on the microenvironment of the active center, changes its electronic

configuration, and optimizes its catalytic activity. Taking the M–N–C configuration as an example, the prevalent M–N_4 structure features a moderate electron cloud density at the metal center, striking a balance between reactant adsorption and desorption, which endows it with excellent Fenton-like catalytic activity. Although the popular M–N_4 configuration has exhibited satisfactory improvements in Fenton-like reactions, the symmetric planar configuration results in an evenly distributed electron density, which impedes the adsorption and activation of reactants, ultimately compromising catalytic efficiency. Recently, numerous studies have proven that decreasing the coordination number of SACs can enhance their electron-donating ability, optimize electronic structures, and reduce steric hindrance of the catalyst, thus accelerating PMS activation.[93,94] Additionally, the unsaturated metal active sites strengthen the interaction with PMS, altering the generation pathway of ROS. For instance, Liang *et al.* fabricated a series of atomically dispersed cobalt catalysts with different coordination numbers (Co–N_x) (Fig. 3a–d).[95] It was discovered that the reduction of coordination number of Co sites led to the increase of electron density of the single Co atom in Co–N_x to promote the reduction of PMS, which governed the Fenton-like performance of Co–N_x, and also reduced pyridinic N-coordinated C atoms, weakening PMS oxidation and decreasing $^1O_2$ production from Co–N_3/PMS to Co–N_2/PMS. Lin *et al.* highlighted the unparalleled superiority of FeN_2 SACs in governing the formation and oxidation behavior of Fe^{IV}=O, as opposed to FeN_3 and FeN_4 configurations (Fig. 3e–g).[96] DFT calculations revealed that FeN_2 sites exhibited a more robust adsorption affinity towards PMS and a decreased energy barrier for the formation of Fe^{IV}=O.

Although decreasing the coordination number is a prevalent strategy in many studies to modulate electronic structures and raise the adsorption energy of PMS on the single sites, as is well known, it inevitably causes a significant decline in the desorption of PMS-derived intermediates and the reconstruction of reactive sites, which in turn impairs the stability and selectivity of SACs. Therefore, Du *et al.* constructed a biochar-based carbon support rich in microporous structures and defects to allow for more nitrogen doping and anchoring of Fe single atoms, forming the high-coordination FeN_5 configuration (Fig. 3h).[97] Compared with the FeN_4 site, the FeN_5 sites demonstrated a more favorable global energy profile, for example, moderate adsorption energy for PMS and a d-band center relatively far from the Fermi level. The axial ligand of the FeN_5

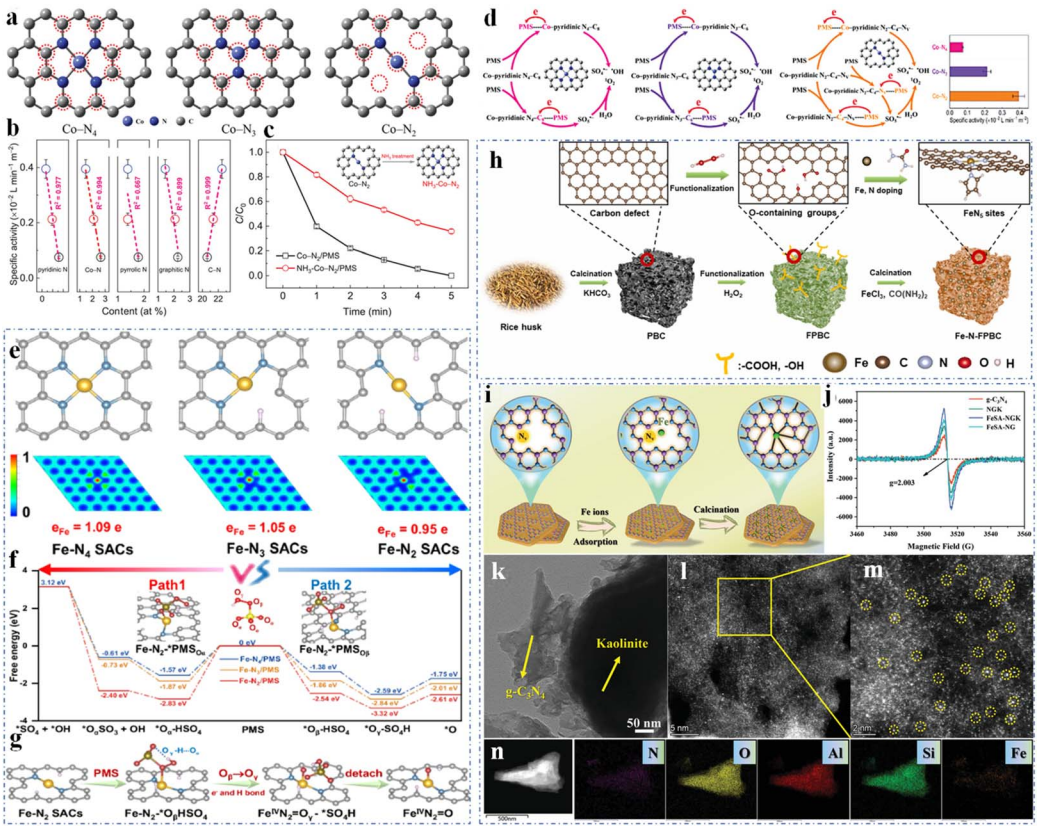

Fig. 3 (a) Co–N_x catalysts with different coordination numbers. (b) Correlations between activity and contents of different N species and C–N. (c) Catalytic activity comparison of Co–N_2 before and after NH_3 treatment. (d) PMS conversion mechanism over Co–N_x. Copyright 2022, Wiley-Advanced. (e) The structure models and electron density distribution images of Fe–N_x SACs. (f) Free energy of the possible reaction paths in different adsorption sites. (g) The paths for the reaction of PMS and Fe–N_2 SACs. Copyright 2024, Springer Nature. (h) Synthesis process of a porous biochar-based SAC with FeN_5 sites (Fe–N–FPBC). Copyright 2024, Elsevier. (i) The synthesis processes of an FeSA–NGK composite. (j)–(n) solid-state EPR spectra, TEM images, atomic-resolution HAADF-STEM image and corresponding EDX mapping of the FeSA–NGK composite. Copyright 2022, Wiley-VCH.

thermodynamically promoted electron transfer from contaminants to the catalyst, and also enabled smoother SO_4H desorption, thus facilitating active site regeneration. Wu's group prepared the highly coordinated CoN_5O_1 catalyst and found that the five-coordinated structure (CoN_5O_1) formed by oxygen doping significantly enhanced the activity by optimizing the PMS adsorption energy and reducing the formation energy barrier of Co(IV)=O. In contrast, the low-coordination CoN_3O_2 led to a decrease in electron transfer efficiency and a decline in the activation performance of PMS due to the weakening of the coordination field.[98]

Most studies on the regulation of high coordination involve the axial connection of ligands, but the core difference between high coordination and axial coordination lies in the dimensions and symmetry of the coordination structure. High coordination tends to stabilize active centers through multi-atomic synergy, while axial coordination focuses on breaking the electronic symmetry of planar structures to form unique active sites.[99] This structural difference directly affects the activation pathway of PMS by the catalyst and the generation efficiency of ROS in Fenton-like reactions. Zhang *et al.* used kaolinite as a carrier to support g-C_3N_4 and Fe single atoms. The obtained FeSA–NGK composites possessed a high Fe loading and rich N vacancy defects (Fig. 3i–n).[100] The Fe atom coordinated with five N atoms ($Fe–N_5$) and was adjacent to an N vacancy, which regulated local electron density, altering the Fe coordination environment to expose electron channels and lower the energy barriers for $^1O_2$ generation. Such configurations enhanced carrier separation kinetics, enabling excellent organic degradation performance in the PMS/vis system. In fact, it is relatively difficult to prepare highly coordinated configurations with five or more N atoms in the carbon-based single-atom plane. The traditional pyrolysis method cannot precisely control the pyrolysis conditions, resulting in an uneven coordination environment and making directional synthesis difficult. High temperatures can easily cause the removal or rearrangement of N atoms. Although some studies have obtained highly coordinated structures through special crystal growth or secondary atom doping strategies,[83] there is still a gap from regular planar multi-N doping. At present, research mainly focuses on optimizing the synthesis methods. In the future, it will be necessary to explore innovative paths and control means to achieve the preparation of stable and high-proportion planar high-coordination configurations.

3.1.3 Axial coordination. As an emerging coordination regulation strategy, axial coordination refers to the coordination of ligands with a single atom along a direction perpendicular or non-coplanar to the plane where the center of the active single atom lies. Many advanced studies have achieved flexible adjustment of the electronic structure of metal single atoms by rationally designing axial ligands, making it more conducive to the adsorption and activation of reactants, thereby enhancing the activity of catalytic reactions.[99,101–104] Changing the types of axial ligands will lead to changes in the adsorption mode and reaction path of reactants on the surface of metal single atoms, thereby achieving the regulation of reaction selectivity. In addition, the axial coordination strategy also plays a significant role in stabilizing the loss of active centers during the reaction and enhancing the stability of the catalyst.

Up to now, ligands involved in the axial coordination of SACs have included those containing N, C, O, P, S, and halogen atoms.[53,105–108] Liu *et al.* fabricated an Fe_1/C_3N_4 SAC ($Fe–N_5$) with axial nitrogen coordination for enhanced Fenton-like reaction (Fig. 4a).[34] Axial nitrogen disrupted the symmetry of the original planar structure of $Fe–N_x$ sites, altering H_2O adsorption behavior on $Fe–N_5$ without affecting H_2O_2 activation. Similarly, Fu *et al.* revealed that axial five-coordinated Fe SACs displayed outstanding catalytic performance in phenol oxidation, as a result of the modulated electronic state of Fe atoms and the decreased activation energy of H_2O_2 caused by axial coordination (Fig. 4b).[109] Gu *et al.* developed archetypal CoN_4 and CoN_4S models to elucidate the fundamental impetus for PMS activation and the formation of Co(IV)=O induced by axial S coordination (Fig. 4c).[110] They found that the cooperation of axial S altered electron distribution within the 3d orbitals of Co and weakened the adsorption between the Co site and PMS. Moreover, the d-band center of Co in CoN_4S was also far from the Fermi level compared with that in CoN_4. Considering that strong interactions could poison the active sites and inhibited the desorption of PMS, such a moderate adsorption instead showed superiority in the desorption of PMS. The CoN_4S–PMS* complex exhibited a relatively narrow d-band that was closer to the Fermi level and a greater orbital overlap between Co 3d and O 2p. The enhanced CoN_4S–O interaction upon PMS adsorption lowered the energy barrier for Co(IV)=O formation and improved charge-transfer efficiency to PMS. Shen *et al.* simultaneously doped P and S atoms into the Cu SACs in the planar and axial positions respectively to obtain CuSA/CN–P&S and achieved a synergistic regulation (Fig. 4d and e).[111] The axial S coordination raised the d-band center and widened the e_g^* orbital of Cu, enhancing the adsorption selectivity for the terminal oxygen of PMS. Simultaneously, planar P coordination notably boosted electron transfer efficiency by generating an intrinsic electric field within the carbon skeleton. In addition, Wang's group designed a dual-atom $FeCo–N_4O_1C$ catalyst, in which Fe and Co atoms were bridged by two-dimensional planar N atoms and a three-dimensional (3D) axial O atom (Fig. 4f).[105] This architecture induced a spin-state transition of Fe from a low-spin to an intermediate-spin configuration, and enabled optimal adsorption/desorption of reaction intermediates, thereby decreasing the energy barriers for the generation of $^1O_2$ and high-valent Co–oxo species during PMS activation. Halogens have recently been innovatively used as axial ligands to regulate the coordination environment of the metal center of M–N–C, break the symmetry of the planar coordination environment and reshape the electronic structure and geometric configuration of the active site, thereby achieving the regulation of the catalytic activity and selectivity of SACs. The electronegativity disparity between halogens and other ligands allows axial coordination to synergistically tune the electronic structure of the metal atom, adjust the d-band center, and optimize reaction intermediate adsorption energies. Wang's group synthesized a graphene-supported single-atom catalyst featuring atomically dispersed FeN_4Cl sites (Fe–N/Cl–C) (Fig. 4g).[112] Their findings

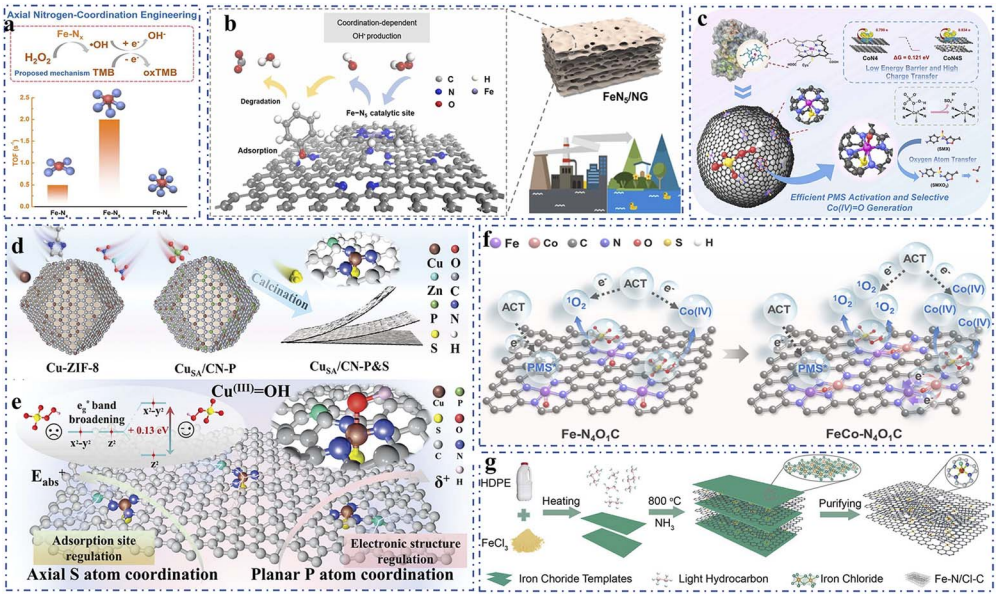

Fig. 4 (a) Axial nitrogen-coordination engineering strategy in Fe_1/C_3N_4 SAC (Fe–N_5). Copyright 2023, Elsevier. (b) Axial coordination tunes Fe SACs for boosting H_2O_2 activation. Copyright 2023, Elsevier. (c) The selective generation of high-valent metal–oxo species induced by CoN_4S–CB. Copyright 2024, Elsevier. (d) The preparation of CuSA/CN–P&S. (e) The mechanism of multitype coordination synergistically regulating CuSA/CN–P&S activation of PMS to Cu(III)=OH species. Copyright 2024, Wiley-VCH. (f) The catalytic pathways for Fe–N_4O_1C and FeCo–N_4O_1C. Copyright 2024, American Chemical Society. (g) The preparation of Fe–N/Cl–C. Copyright 2025, Wiley-Advanced.

showed that the axial introduction of chloride delicately adjusted the local electronic structure of FeN_4 sites by altering the electron filling of Fe 3d e_g orbitals in the d_{z^2} orientation, which in turn enhanced PMS activation *via* the increased conductivity of carbon supports and facilitated PMS adsorption on the FeN_4Cl site. Meanwhile, they also constructed a multi-dimensional Co-SAC (Co_1CNCl/S) with axial Cl and second-shell S.[113] This configuration shifted the d-band center of active Co sites downwards, enhanced charge-transfer, and strengthened the Co–O interaction with PMS. It formed a surface electrophilic intermediate with mild oxidation potential to trigger the non-radical electron-transfer pathway. Despite progress in halogen atom coordination for SACs, challenges remain. Halogen stability under reaction conditions, especially in high-temperature or extreme pH environments, and precise control of the structure–activity relationship are key hurdles. Future research should prioritize developing stable coordination strategies, integrating advanced characterization with theoretical calculations to elucidate catalytic mechanisms, and advancing practical applications in energy and environmental sectors.

3.2 Support-effect modulation

In SACs, the single-atom sites are isolated and evenly distributed on the supports through chemical bonding with support elements. This unique structure endows SACs with adjustable metal active sites and strong metal–support interactions (MSIs). The properties and structure of the supports exert a substantial influence on the regulation of the microenvironment of single atomic centers in terms of catalytic activity of SACs, the efficiency and pathway of ROS generation, the adsorption and activation of reactants, and the stability of the catalyst. This subsection will comprehensively summarize the latest advancements in support-effect modulation, delving into how support effects impact the catalytic performance and reaction mechanism of SACs in Fenton-like reactions, including the characteristics of different support materials and the MSIs.

3.2.1 Carbon supports. To date, SACs supported by carbonaceous materials remain the research mainstream because of the rich anchoring sites and superior surface adsorption capabilities of carbon materials, which enable the stabilization of single metal atoms. The most common carbon supports include one-dimensional (1D) carbon nanotubes (CNTs),[43,114] two-dimensional (2D) graphene oxide (GO) and graphene-like layered carbon,[44,115] graphitic carbon nitride ($g\text{-}C_3N_4$),[116,117] metal–organic framework (MOF)-derived three-dimensional (3D) porous carbon, biomass-derived porous carbon, *etc.* (Table 1).[118,119] Furthermore, various regulation methods including heteroatom doping, introduction of defects, and grafting of functional groups can be utilized to precisely modulate the binding force between metal and carbon supports, thus governing the catalytic activity of SACs in Fenton-like reactions (Fig. 5a). For example, Ajayan's review summarized the latest research advancements in optimizing the electronic structures of metal active centers in carbon-based SACs through the introduction of polynary metal and multi-heteroatom doping strategies.[120] Some researchers have particularly focused on heteroatom doping in the second coordination shell of single atoms to modulate their electronic structures, thereby investigating the optimization mechanisms of catalytic performance and reaction pathways.[92,121,122]

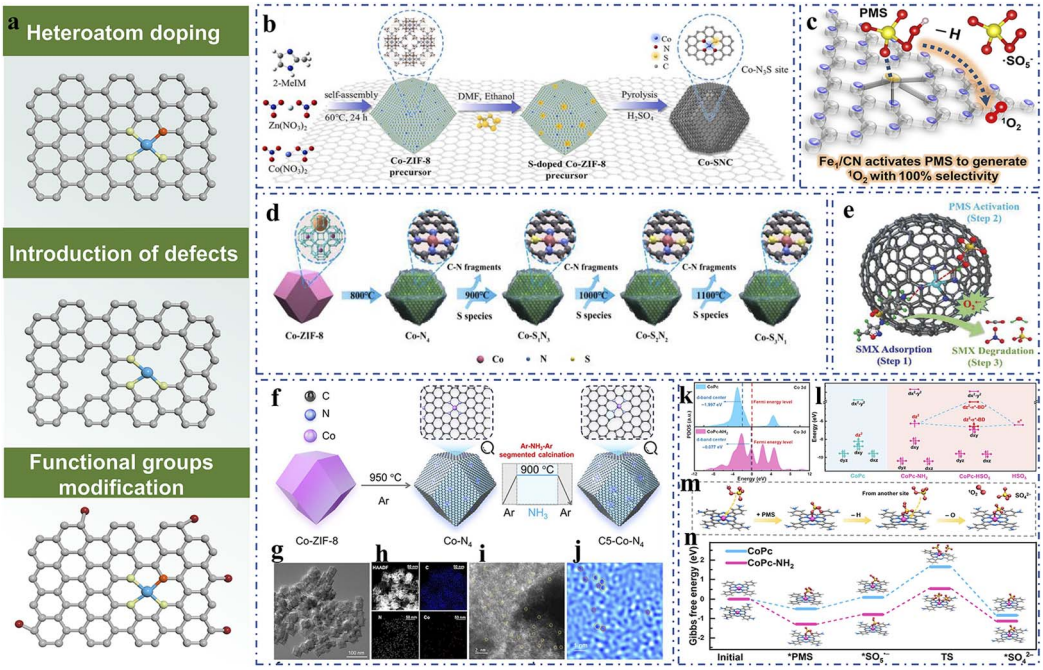

Fig. 5 (a) The regulation strategies of carbon supports. (b) The preparation procedure of the Co–SNC catalyst. Copyright 2023, Elsevier. (c) PMS activation process by Fe_1/CN. Copyright 2021, Wiley-VCH. (d) The preparation procedure of Co–S_xN_{4-x}. Copyright 2024, Springer Nature. (e) The degradation mechanism in the Fe–N_4–PC-2/PMS system. Copyright 2021, Wiley-Advanced. (f) The synthesis of Co–N_4 and C5–Co–N_4. (g) HRTEM image of C5–Co–N_4. (h) HAADF-STEM images and corresponding EDS maps of C, N, and Co. (i) AC-STEM image of C5–Co–N_4. (j) Fourier transform fitting results of C5–Co–N_4. Copyright 2025, Wiley-Advanced. (k) PDOS of Co 3d in CoPc and CoPc–NH_2. (l) Energy levels of the Co 3d orbital and orbital interactions between PMS and CoPc–NH_2. (m) Reaction pathways of PMS activation at Co–N_4 sites, and (n) the corresponding Gibbs free energy (eV). Copyright 2023, American Chemical Society.

Although doping heteroatoms such as nitrogen (N), sulfur (S), phosphorus (P), boron (B), and oxygen (O) and introducing atomic defects, including nitrogen-vacancy,[123,124] oxygen-vacancy,[125,126] and carbon-vacancy,[127,128] have been widely applied to regulate the electronic structure of the metal center in SACs, the exact governing principles remain debatable. Moreover, even with the same regulatory approaches and the same coordination environment of active metal sites, there are marked differences in the electronic structures and catalytic behavior of metal centers. In Zhang's study, the Co atom in the Co–SNC catalyst featuring Co–N_3S sites exhibited a +2 valence state (Fig. 5b).[80] In contrast, the Co–CGBC in Cui's research showed a significant decline of the Co oxidation state due to the coordination of Co with S atoms.[129] The same phenomenon was also emphasized by Pei *et al.* (Fig. 5d).[130] They noted that after S doping in Co SACs, the active configuration changed from CoN_4 to CoS_1N_3, leading to a notable reduction in the valence state of Co. Additionally, while both studies utilized FeN_4 as the dominant active site, distinct catalytic behaviors were observed. Zhang *et al.* developed an Fe single-atom catalyst (Fe_1/CN) supported on CN, where the FeN_4 sites exclusively activated PMS to generate 100% $^1O_2$ for selective pollutant degradation (Fig. 5c).[131] In contrast, Peng's group designed an Fe–N–PC catalyst with single Fe atoms anchored on porous N-doped carbon, demonstrating that multiple ROS coexisted and synergistically enhanced pollutant degradation efficiency (Fig. 5e).[132] These comparative results highlight the critical role of the support architecture and coordination environment in tuning ROS selectivity and catalytic pathways. In view of this, Ouyang's team pointed out that defects on the carbon supports were an important part that could not be ignored when evaluating the structure–activity relationship of SACs in Fenton-like systems.[133] Recently, they applied a pyridinic N etching approach to precisely create pentagon defects in CS-SACs (C5–Co–N_4) (Fig. 5f–j). The newly formed pentagon defects raised the Co d-band center and enhanced electron density in the d_{xz} and d_{z^2} orbitals. As a result, electron transfer between the Co atom and PMS became more efficient. Moreover, the pentagon defect modification also refined the adsorption of intermediate oxygen species, enabling the effective production of $^1O_2$ in the reaction. Their findings provided a meaningful defect-engineering on CS-SAC design and application. The interaction between the metal atoms and the supports can also be regulated *via* functional group modification.[134,135] Lai's group used an amino (–NH_2) functional group modification strategy to regulate the electronic structure of Co sites in a cobalt phthalocyanine/graphene catalyst (CoPc/G–NH_2), which exhibited outstanding catalytic activity in PMS activation (Fig. 5k–n).[135] Amino modification of CoPc/G–NH_2 significantly boosted the electron density around the Co center and caused a positive shift in the d-band center of Co 3d. The decreased electron occupancy was conducive to strengthening the adsorption of PMS and promoting the formation of a reactive PMS* intermediate, thus lowering the activation energy of PMS. In addition, Kohn–Sham molecular

orbitals indicated that the activation of PMS was mainly governed by $3d_{z^2}$ of Co(II) sites and pai* of HSO_5. Amino modification raised the energy of the d_{z^2} orbital and reduced the binding energy of d_{z^2} electrons in CoPc/G–NH_2. These electronic structure changes endowed CoPc/G–NH_2 with enhanced electron-donating ability, which in turn facilitated more efficient activation of PMS.

3.2.2 Carbon nitride (CN) supports. Two-dimensional carbon nitride (CN) with well-defined C and N sites and high N content offers abundant and evenly-distributed sites for single-atom fixation. Furthermore, CN demonstrates remarkable chemical stability and cost-efficiency, which further elevates its appropriateness as a support for SACs. Currently, a well-established approach to fabricate SACs supported on CN involves the self-assembly of metal ions with nitrogen-rich carbon-based organic molecules, including melamine,[117,136,160] urea,[159] and dicyandiamide,[161] complemented by pyrolysis. In our prior research, we synthesized Fe-based SACs (Fe/NC–XPVP) with Fe active centers of different sizes by pyrolyzing a homogeneous powdered mixture composed of melamine, PVP and iron nitrate (Fig. 6a).[162] Melamine was initially converted into a g-C_3N_4 support and subsequently transformed into N-doped carbon. In addition to this kind of SAC with CN as the intermediate support, CN has also been widely reported as the final carrier. Zhang *et al.* prepared a single-atom Fe catalyst using g-C_3N_4 as the support (Fe_1/CN). They converted the traditional Fe_1–N_4 into Fe_1–C_2N_1 by acid etching (Fig. 6b–d).[163] It is widely recognized that the coordination environment surrounding the metal centers has a profound impact on the distribution of the bonding orbitals within the 3d orbitals of metal atoms. The energy levels of metal d-orbitals can strongly interact with the highest occupied molecular orbitals (HOMOs) and lowest unoccupied molecular orbitals (LUMOs) of adsorbates on the surface. This interaction is pivotal, as a greater electron density

Table 1 Application details of carbon-supported SACs in Fenton-like systems[a]

	Sample	Support origins	Modulation method	Active sites	Main ROS	Ref.
1D	Cu/V_{550}–TCN	Urea, melamine	ID	Cu–N_3 and C_V	$^1O_2$	127
	SAAg@PTCN	Urea, melamine	HD	SAAg@PTCN	$^1O_2$, $^{\bullet}O_2^-$	136
	Co–N_3O_1	Melamine	HD	Co–N_3O_1	$^1O_2$	116
	FCC-5	Fe-MOF, melamine	FM	Fe atoms	$^{\bullet}$OH and ETP	114
	CoSCN	Urea, melamine	HD	CoN_3S	Co(IV)=O	137
	Pd–F/SCNT	CNT powders	HD	Pd atoms	$^{\bullet}$OH, $^1O_2$	138
2D	Co–*x*P–C_3N_5	3-Amino-1,2,4-triazole, HCCP	HD	P–N–Co bonds	$SO_4^{\bullet-}$, $^{\bullet}$OH	121
	FeCN–N_v-2	Dicyandiamide	ID	Fe–N_4 and N_V	$^1O_2$, $^{\bullet}O_2^-$	124
	CoPc/G–NH_2	Graphene	FM	Co–N_4	$^1O_2$	135
	FeP/Fe_1–GO	GO	HD	FeP and Fe_1–GO	$^{\bullet}$OH and $^{\bullet}O_2^-$	115
	CuBCN	Cyanamide	HD	CuN_3–B	$^1O_2$	139
	PC_vFe_1-5	Glucosamine	ID	Fe–N_4 and C_V	–SO_5H/–SO_4	140
	Co–OCN	Dicyandiamide	HD	CoN_5O_1	Co(IV)=O	141
	Fe–N_4O	Melamine	HD	Fe–N_4O	Fe(IV)=O, ETP	142
	CoN/O–pCN	Urea	HD	CoN_2O_3	$^1O_2$, $SO_4^{\bullet-}$, $^{\bullet}$OH	143
	Fe-NSC-L	Phenanthroline, thiourea	HD	Fe–N_4	Fe(IV)=O	92
	Co@rGO	GO	HD	Co_4S_3	$^1O_2$	144
	Co_{SA}–N–$C_{O,S}$	*p*-PDA	HD	CoN_4	$SO_4^{\bullet-}$, $^1O_2$, $^{\bullet}$OH	145
	Mn_{SA}–N–$C_{O,S}$	*p*-PDA	HD	MnN_4	$^1O_2$	146
	Cu–N_4/C–B	Carbamide	HD	CuN_4	High-valent copper–oxo species	87
3D	Fe–NC_v-900	ZIF-8	ID	Fe–N_4 and C_V	High-valent iron–oxo species	128
	C5–Co–N_4	Co–ZIF-8	ID	Co–N_4 and C_V	$^1O_2$	133
	FeNC	Chitosan	FM	Fe–N_5 and C=O	$^1O_2$, $^{\bullet}$OH and $SO_4^{\bullet-}$	134
	CoNBC600	Sodium alginate	HD	Co–N_3	$SO_4^{\bullet-}$, $^{\bullet}$OH	119
	Co–S@NC	Reed-derived biosorbents	HD	S–Co_3O_4	$^1O_2$, $^{\bullet}O_2^-$, $^{\bullet}$OH and $SO_4^{\bullet-}$	147
	Fe_{SA}–NPS@C	ZIF-8	HD	Fe–N_4	Fe^VN_4=O	148
	Fe–PNC	Fe–ZIF-8	HD	Fe–N_4P_2	ETP	149
	Co–SNC	Co–ZIF-8	HD	Co–N_3S	$^1O_2$, $SO_4^{\bullet-}$, $^{\bullet}O_2^-$, $^{\bullet}$OH	80
	ZIF–CoN_3P–C	ZIF-8	HD	Co–N_3P	$^1O_2$	150
	Fe–SN–C	$Fe(acac)_3$@ZIF-8	HD	Fe–S_1N_3	Fe(IV)=O	151
	SACoN/BCN	Co-MOF	HD	CoN_4	$^1O_2$	152
	Co_{SA}–BNC	Chitosan	HD	CoB_1N_3	Co(IV)=O	153
	Co@NSOC-*T*	Co-MOF	HD	Co, CoO, and Co_9S_8	$^1O_2$, $^{\bullet}O_2^-$	154
	Fe–BNC	ZIF-8	HD	Fe–N_3B	Fe(IV)=O	155
	Co@NPSC	Eggshell powder	HD	CoN_4	$^1O_2$, $^{\bullet}O_2^-$, $^{\bullet}$OH, $SO_4^{\bullet-}$	156
	Fe–N_xB/GCN	Chitin	HD	Fe–N_4–B	Fe(IV)=O	157
	Co@$B_{0.5}$–DB700	Bean dregs	HD	Pyridinic N and B–N	Co(IV)=O, $SO_4^{\bullet-}$	158
	HFeNC–g-C_3N_4	Urea	HD	Fe–N_4	$^1O_2$, $^{\bullet}O_2^-$	159

[a] As for the modulation method, introduction of defects is marked as ID for short, HD stands for heteroatom doping, and FM for functional group modification.

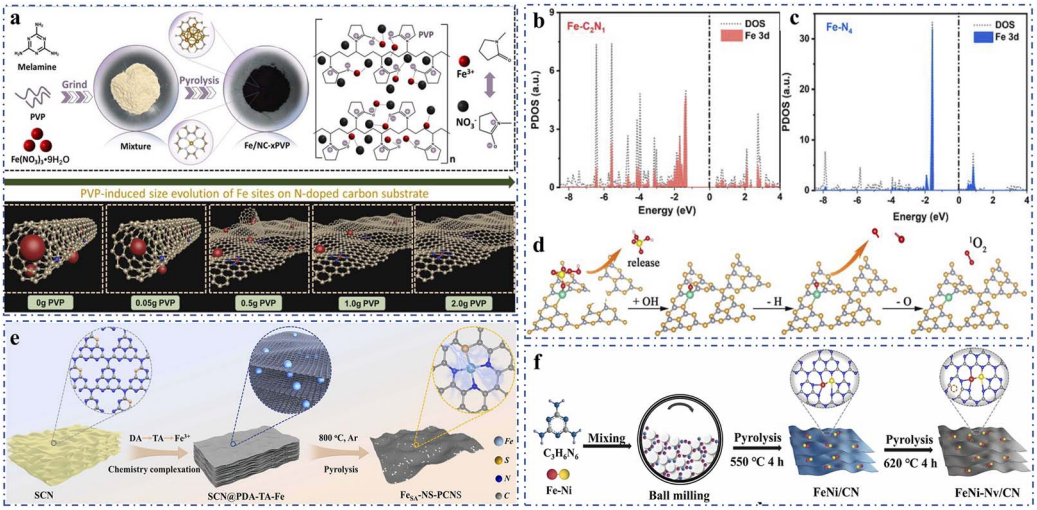

Fig. 6 (a) The preparation of Fe/NC–XPVP. Copyright 2024, Elsevier. (b) and (c) The calculated PDOS of Fe–C_2N_1 and Fe–N_4 respectively. (d) Schematic illustration of the reaction steps for PMS activation to $^1O_2$ on Fe–C_2N_1. Copyright 2022, Elsevier. (e) Synthesis procedure and microstructures for Fe_{SA}–NS–PCNS. Copyright 2024, Elsevier. (f) Schematic synthesis procedure of FeNi–N_v/CN. Copyright 2025, Elsevier.

near the Fermi level enhances the adsorption of reactants, facilitating the catalytic processes. According to DFT results, as compared with FeN_4 sites, the charge distribution around Fe atoms in Fe–C_2N_2 configuration was far from the Fermi level, thus showing a moderate binding force for PMS and a lower energy barrier for $^1O_2$ production. Then, Zhu *et al.* further doped S atoms on CN and used the resulting SCN as a support to load Fe single atoms, realizing asymmetric coordination regulation of the Fe active center. The charge distribution balance around Fe in Fe_{SA}–N_3S_1 was disrupted and underwent a rearrangement, boosting the strong binding force between active sites and PMS, and expediting electron transfer. The direct generation pathway of $^1O_2$ from PMS activation on the Fe_{SA}–N_3S_1 was elucidated (Fig. 6e).[164] As we mentioned above, due to the thermal instability of CN, it is very easy to introduce a large number of C–N vacancy defects into the planar structure of CN as electron trap states, which can induce the coordination of metal atoms with vacancies, thereby forming a high-order coordination structure. For instance, V_N–CoN_3O_1 was reported by Wang *et al.*,[165] and $CNFe_2$-0.6 was reported in Zhu's work.[166] In addition, N-vacancy defect engineering can optimize the valence state and electron transfer ability of metal single atoms. The Fe_1–N_v/CN catalyst, which featured isolated Fe single atoms anchored on nitrogen-vacancy (N_v)-rich C_3N_4 nanosheets, efficiently activated H_2O_2 under visible light irradiation. The N_v defects acted as electron traps, funneling the electrons toward the Fe active sites to enhance their redox reactivity.[123] The FeNi–N_v/CN catalyst synthesized by Qin *et al.* demonstrated exceptional PMS activation performance owing to the synergistic interplay between the enhanced electron density around Fe–Ni atomic pairs and the single-metal active sites coupled with N_v on the catalyst surface (Fig. 6f).[167] Moreover, the unique layered architecture and optimal interlayer spacing of C_3N_4 endowed it with the capability to regulate confinement effects and reaction pathways in catalytic systems. These aspects will be elaborated in the following nanoconfinement modulation section.

3.2.3 Metal oxide supports. In contrast to carbon supports, whose surface structures remain uncontrollable during pyrolysis, thereby inevitably introducing uncertainties into the single-atom coordination environment, metal oxides with well-organized crystalline structures offer several advantages as supports for SACs. The abundant surface reactive sites, such as oxygen vacancies and hydroxyl groups, can interact with single-atom metals, ensuring their stable anchoring and preventing agglomeration. Zhao *et al.* engineered a catalyst wherein single Co atoms were anchored onto CuO with abundant O_V for the activation of PMS (Fig. 7a).[168] The O_V within the CuO matrix not only served to stabilize the supported single Co atoms and augmented their loading capacity but also accelerated electron transfer processes and promoted the generation of $^1O_2$ during the oxidation reaction, thereby enhancing the overall catalytic performance. Yang *et al.* developed TiO_2 with rich oxygen vacancies (O_V) as a support to prepare Fe_1/TiO_2–O_V SACs to investigate their synergistic performance in photo-Fenton phenol degradation (Fig. 7b).[169] O_V remarkably expedited the separation and oriented delivery of photogenerated electrons to Fe_1 single atoms, thereby enabling the rapid generation of ROS and concurrently promoting the selective adsorption and activation of phenol. Additionally, owing to diverse physical properties including magnetism and conductivity, and tunable electronic structure of metal oxides, the catalyst exhibited facile separation and efficient electron transfer capabilities, with the modified electronic state optimizing the catalytic performance.

Xia *et al.* fabricated a porous SAC aerogel, featuring abundant CoN_4 sites anchored on a CoO_x support, to activate PMS for the degradation of *p*-nitrophenol (Fig. 7c–f).[170] Their findings revealed that CoN_4 acted as the dominant activation site, exhibiting a moderate binding energy with PMS. Meanwhile, the CoO_x nanoparticles substantially enhanced the adsorption

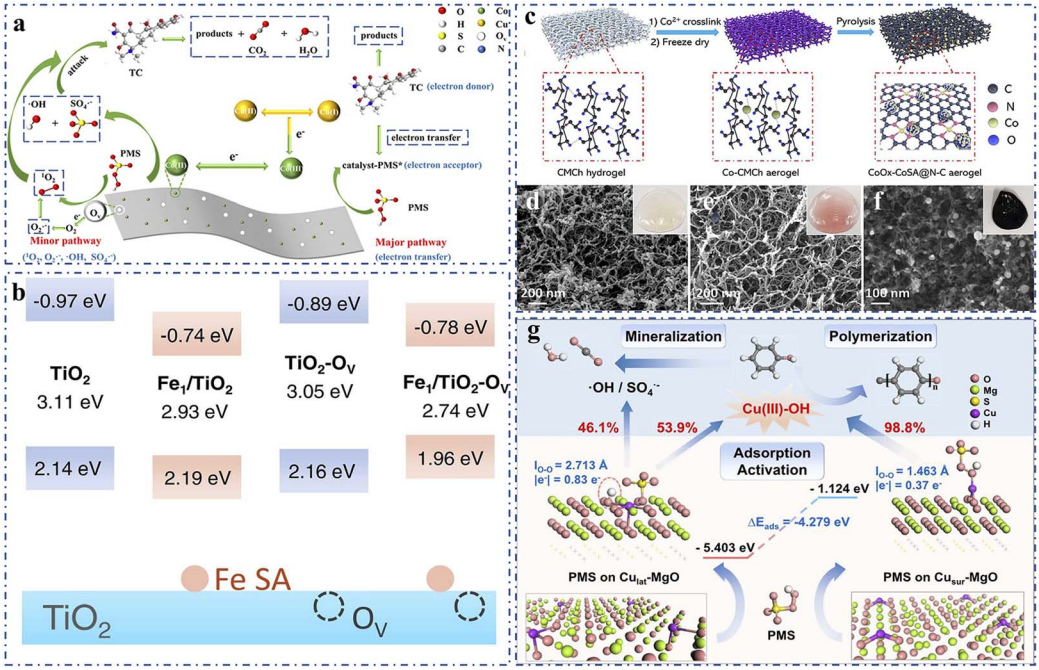

Fig. 7 (a) PMS conversion mechanism over Co_{NP}–CuO. Copyright 2023, Elsevier. (b) Band edge alignments of Fe_1/TiO_2–O_V, Fe_1/TiO_2, TiO_2–O_V and TiO_2 samples. Copyright 2024, Elsevier. (c) Schematic diagram for the formation of CoO_x–CoSA@N–C aerogel; SEM images of (d) CMCh hydrogel, (e) Co–CMCh and (f) CoO_x–CoSA@N–C aerogel. Copyright 2024, Elsevier. (g) Adsorption and activation of PMS on the Cu-lat/Cu-sur sites of Cu SACs and the routes of PMS conversion and contaminant degradation. Copyright 2025, American Chemical Society.

capacity of the catalyst for target pollutants. Density functional theory (DFT) calculations elucidated that the integrated CoO_x species could instigate a reconfiguration of the electronic distribution at the CoN_4 active sites, which gave rise to an electron-enriched environment around the Co center and concurrently generated electron-depleted states on the N atoms. Such an electronic restructuring induced the synergy of CoO_x and CoN_4, and lowered the d-band center of the composite, thus optimizing ROS desorption and enhancing reaction kinetics. Recently, Liu *et al.* selected magnesium oxide (MgO) as a structurally robust support for anchoring single copper (Cu) atoms to facilitate a PMS-mediated Fenton-like reaction (Fig. 7g).[171] By strategically adjusting the spatial configuration of Cu atoms from lattice-embedded to surface-anchored states, the catalytic system underwent a paradigm shift in reaction pathways toward a predominant polymerization transfer (PT) pathway, leading to a substantial enhancement in contaminant degradation efficiency. Despite the significant progress in leveraging metal oxides as supports for SACs in many catalytic reactions, the metal oxide-based SACs applied in Fenton-like reactions are relatively few. Metal oxides with diverse structural characteristics, including surface defects, crystalline phases, and coordination environments, play pivotal roles in determining the catalytic performance. Therefore, a comprehensive understanding of how these structural features precisely modulate Fenton-like activity and reaction mechanisms is still needed.

3.2.4 Porous material supports. Porous materials, with their unique pore structure, high specific surface area and controllable surface properties, have become important supports for optimizing the performance of SACs.[172] As we mentioned above, nitrogen-rich and hierarchical MOFs are the predominantly utilized precursors that can be transformed into metal and nitrogen atom co-doped SACs featuring a three-dimensional carbon substrate through pyrolysis followed by post-treatment processes.[173–177] This is primarily ascribed to the well-organized architectures and numerous uncoordinated metal active centers of MOFs. The obtained SACs with adjustable porous structure can provide favorable diffusion and transport channels for reactant and product molecules, enabling the substrate to fully approach the active site and enhancing the efficiency of the Fenton-like reactions. In addition, the porous structure and ligand-anchoring functionalities of MOFs render them directly applicable as SAC supports.[178,179] Using a multipyrazole benzene ring-based ligand, Zhou and colleagues engineered three transition metal-neutral single-atom MOF catalysts featuring an M–N_4–C coordination structure (Fig. 8a–j).[180] Theoretical calculations demonstrated that Co-MOF outperformed Cu-MOF and Zn-MOF in electron transfer kinetics. Moreover, the introduction of vacancies in Co-MOF was found to facilitate $^1O_2$ generation by lowering the associated activation energy barriers. Covalent organic frameworks (COFs) are also an ideal platform for incorporating highly dispersed metal single atoms with high loading and well-defined structures, owing to their excellent structural designability and periodic coordination microenvironment. More critically, the coordination environment of metal atoms can be accurately tailored *via* COF structural design, thus adjusting their photogenerated charge separation ability to promote PMS

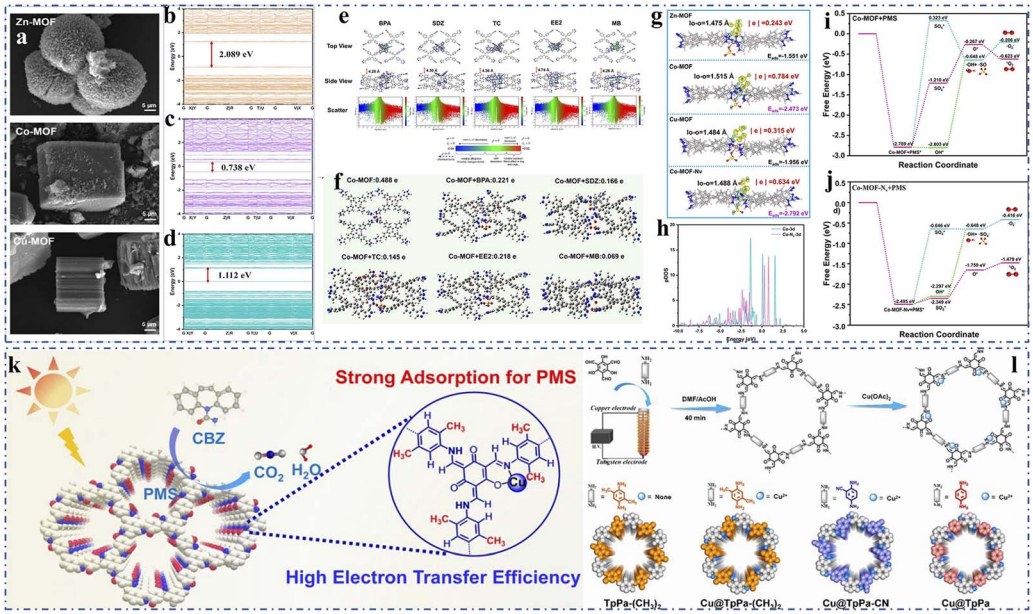

Fig. 8 (a) SEM images of three types of MOFs. Band structure of (b) Zn-MOF, (c) Co-MOF, and (d) Cu-MOF. (e) The interaction forces between Co-MOF and five pollutants. (f) Charge transfer of Co-MOF adsorption on five pollutants. (g) Binding of the three types of MOFs and Co-MOF–Nv with PMS. (h) Density of states of Co-MOF and Co-MOF–Nv. Intermediates of (i) Co-MOF and (j) Co-MOF–Nv activated PMS and energy barriers for generating various ROS. Copyright 2025, Elsevier. (k) CBZ mineralization mechanism over Cu@TpPa–$(CH_3)_2$. (l) The preparation of TpPa–$(CH_3)_2$ and single-atom Cu anchored on TpPa–X. Copyright 2024, Royal Society of Chemistry.

activation.[181,182] For instance, a ketoenamine-based COF was employed as a support to fabricate a Cu single-atom catalyst (Cu@TpPa–X), which served as an efficient PMS activator for the photocatalytic degradation of carbamazepine (CBZ) (Fig. 8k and l). The coordination microenvironment of Cu sites was precisely customized at the atomic level by introducing different functional groups. The resulting Cu@TpPa–$(CH_3)_2$ had a high Cu loading content (5.8 wt%) and exhibited good mineralization efficiency of CBZ.[181] To date, SACs supported by MOFs or COFs have been primarily explored in hydrogen evolution and some electrocatalytic applications. However, their utilization in Fenton-like systems for pollutant degradation remains underexplored. Moreover, the molecular-level regulation of SAC microenvironments *via* COF supports, particularly to modulate reactive ROS generation has not yet been investigated. Future research on MOF/COF-based SACs should focus on developing new design strategies by precisely tailoring ligand structures, pore sizes, and functional groups to enable precise anchoring of single-atom active sites and optimize their electronic structures. This will enhance oxidant activation efficiency and ROS generation capacity in Fenton-like reactions. Additionally, integrating *in situ* characterization with theoretical calculations to analyze the impact of support microenvironments on single-atom performance will facilitate practical applications in environmental governance.

3.2.5 Synergistic interaction between supports and single sites. The catalytic performance and stability of SACs in Fenton-like reactions are highly dependent on their microenvironment, especially the interaction with the supports, which not only provide stable anchoring sites for metal atoms to prevent their aggregation, but can also regulate the electronic structure, geometric configuration and reaction microenvironment of metal sites through their synergistic effect, thereby significantly influencing the overall performance of the catalyst. Yu's group employed zinc oxide (ZnO) as the foundation to construct nano-island-structured Co SACs ($Co_{SA/Zn.O}$–ZnO) (Fig. 9a–j).[183] They managed to overcome the compromise between the activity and stability of PMS activation by means of an "island-sea" synergy. In this spectacular system, the small ZnO nanoparticles, acting as the "islands", were employed to restrict and stabilize individual Co atoms, and the extensive ZnO substrate, which served as the "sea", maintained a neutral micro-environment, achieving a synergistic effect. In carbon-based SAC-mediated Fenton-like reactions, defects and functional groups on the carbon support can activate PMS and synergize with metal centers to drive the catalytic process. Nevertheless, most studies predominantly emphasized the pivotal role of metal active sites while neglecting the support's structural variations. Liu *et al.* innovatively achieved the long-range electronic rearrangement of the sp^2 conjugated structure of the carbon support by regulating the dispersion of Fe and Co atoms, inducing the formation of abundant electron-rich regions for PMS attachment, thereby triggering the electron transfer process (Fig. 9r and s). Further studies were conducted to evaluate the synergistic effect of the carbon support in the Fenton-like reaction and its regulatory role in the oxidation pathway.[184] This study overturns the traditional view that the support is merely an "inert substrate", thereby revealing the complex cooperative catalytic network between the support and the active site. In addition, Wei *et al.* constructed carbon vacancies near a single Fe–N_4 site, which

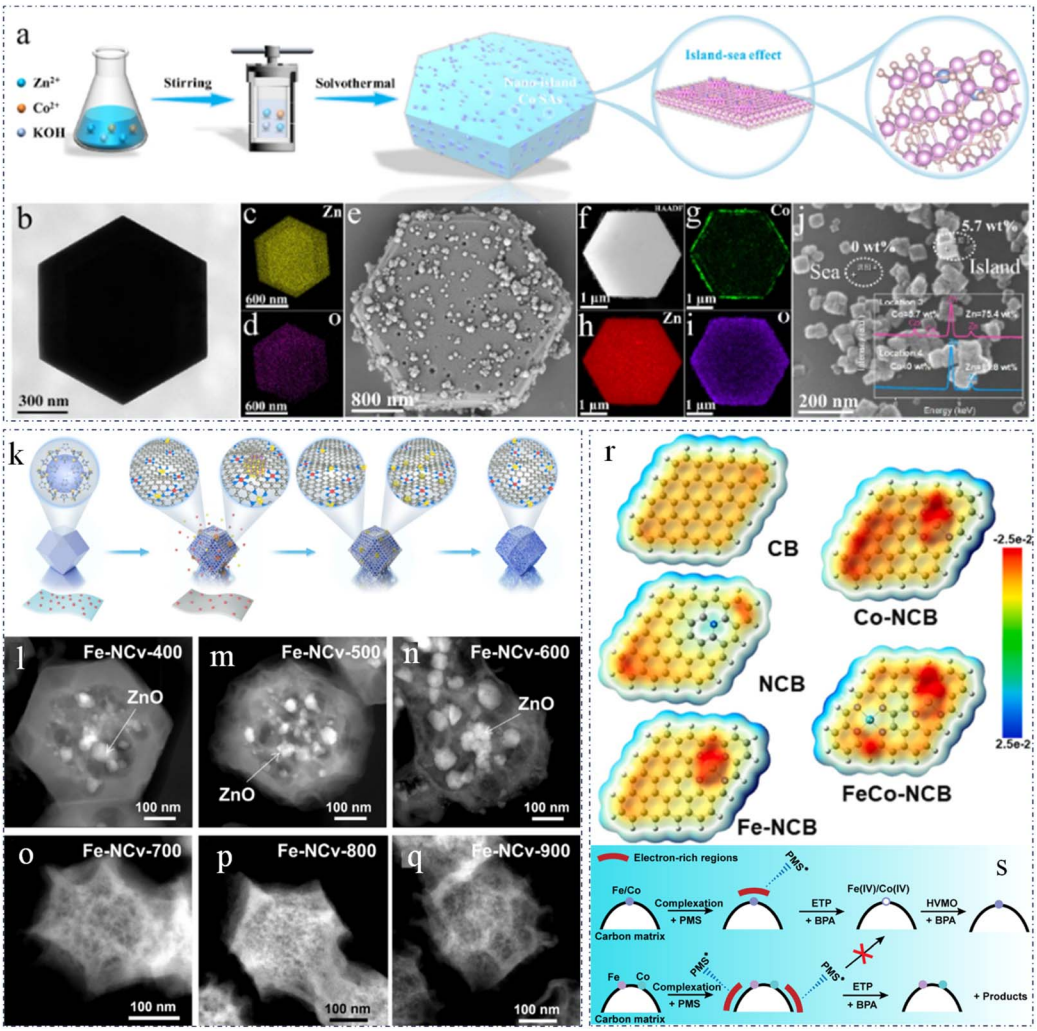

Fig. 9 (a) Synthesis procedure of $Co_{SA/Zn.O}$–ZnO. (b)–(d) TEM image and corresponding element mapping of ZnO. (e) SEM image of $Co_{SA/Zn.O}$–ZnO. (f)–(i) HAADF-STEM elemental mapping of $Co_{SA/Zn.O}$–ZnO. (j) SEM image of small particles on the surface of $Co_{SA/Zn.O}$–ZnO. Copyright 2025, Springer Nature. (k) Schematic illustration of the self-carbon-thermal-reduction strategy. (l)–(q) HAADF-STEM images of Fe–NC_V catalysts at different temperatures. Copyright 2023, Springer Nature. (r) ESP distributions of CB, NCB, Fe–NCB, Co–NCB, and FeCo–NCB. (s) Schematic illustration of the regulated pathway in the FeCo–NCB/PMS system compared to the Fe–NCB/PMS and Co–NCB/PMS systems. Copyright 2024, Elsevier.

had been proven to be beneficial for the formation of C–O bonds and the reduction of the energy barrier in rate-determining steps during the degradation of phenol (Fig. 9k–q).[128] The catalyst ($FeNC_v$-900) with carbon vacancies exhibited significantly enhanced performance compared to FeNC-900 without carbon vacancies. These findings highlight that supports can dynamically couple with single metal sites *via* structural and electronic modulation, forming an integrated catalytic system. Future efforts should focus on establishing structure–activity correlations, developing multi-scale characterization tools to decipher synergistic mechanisms, and providing theoretical frameworks for the rational design of high-performance SACs. Overall, the regulatory mechanisms regarding the support effect in the microenvironment of SACs mainly fall into three aspects: the first is the remodeling of the electronic structure of metal atoms, that is, by precisely regulating the type and structure of the supports to significantly change the valence state distribution and the d-band center position of the single atom, promoting the strong interaction between the metal and the support and the charge transfer between the support and the metal center, thereby optimizing the adsorption and activation of the reactive intermediate, endowing the catalyst with high catalytic activity, and ingeniously changing the reaction path and regulating the reaction mechanism. Secondly, leveraging the pore structure of the support and the modification effect of surface functional groups can accelerate the mass-transfer process of the reaction. This not only enhances the adsorption affinity of the catalyst for reactants but also improves the diffusion efficiency, thereby increasing the reaction rate. Finally, by constructing confinement reaction space and chemical anchoring (covalent/coordination bonds), the interaction between the support and single atoms is strengthened, preventing the agglomeration and

loss of single atomic sites during the reaction, thereby enhancing the stability of the catalyst.

3.3 Spatial confinement modulation

Spatial confinement is an important means to optimize the microenvironment of SACs. On one hand, the interaction between the supports and the single atoms in the confined space will change the electronic structure of the metal centers, affect the charge distribution, adjust the position of the d-band center, and thereby optimize the adsorption and activation ability of the reactant molecules.[185] Moreover, limited reaction space can significantly enrich the reactants near the active centers to accelerate diffusion of reactants and enhance the reaction rate. On the other hand, by confining the configuration and generation pathway of highly active intermediates, the restricted space can enhance their stability, and thereby facilitate the generation of ROS and promote the degradation of pollutants in Fenton-like reactions.

According to the dimensions and structural characteristics of the confined space, the confined effect can be classified into 1D confine (nanotubes, nanowires, *etc.*), 2D confine (sandwich structure of layered materials), and 3D confine (channel structure of porous materials) (Fig. 10).[186–190] 1D nanoconfined spaces are generally embodied by nanotubes or nanochannels, which are distinguished by their prominent high aspect ratios. Carbon nanotubes, first identified in 1991,[191] stand out as one of the most intensively explored substances featuring these 1D nanoconfined spaces. Yang *et al.* confined Co single atoms in a B, N co-doped defective carbon nanotube (Co–B,N-CNT) reactor *via* spatial isolation and dopant-assisted immobilization strategies and applied it in an electro-Fenton reaction to degrade organic pollutants (Fig. 11a–d).[192] The superior catalytic activity of Co–B,N-CNTs could be attributed to the evenly distributed Co single-atom catalysts with abundant defect sites, with the electronic structure precisely tuned by modification of various electronegative atoms, and the advantages of hollow nanotube architecture.

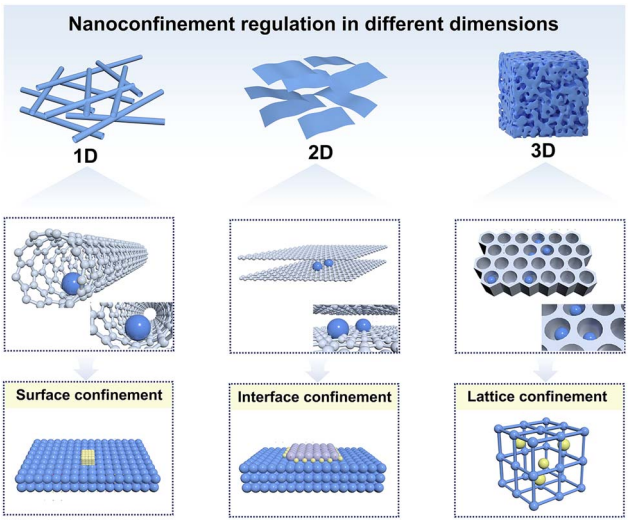

Fig. 10 Schematic illustration of nanoconfinement regulation in different dimensions.

Layered 2D materials hold significant promise for constructing a 2D confined space with intrinsic interlayer regions characterized by van der Waals interactions.[193,194] The distribution of metal atoms on the surface is relatively uniform, and the active sites are fully exposed, which is conducive to the contact and reaction between reactant molecules and active metal sites. Recently, Jiang *et al.* developed an angstrom-scale confinement strategy to fabricate a cobalt (Co) and manganese (Mn) dual-atom catalyst (Fig. 11e).[195] In this design, Co and Mn atoms were anchored on a flexible 2D carbon nitride interlayer. This unique structure precisely regulated the atomic coordination, thereby enabling the spin state of the metal center to be dynamically modulated within the angstrom-scale confined space. Based on characterizations and DFT calculations, the authors revealed the reaction mechanism. Specifically, PMS adsorption on Co–Mn bimetallic sites drove medium spin Co in Co–N_4 to absorb electrons and break the O–H bond of PMS, generating *SO_5. The generated *SO_5 increased the interlayer distance, decomposed Co–N and Mn–N, and shifted spin states from medium to high spin. Then, Co and Mn in the high-spin state extracted *O_2 from *SO_5 and reverted to the medium spin state. Relative to the non-enclosed space, this flexible spin state alteration amplified the generation of $^1O_2$ by 38.6 times. Layered double hydroxides (LDHs) have positively charged hydroxide layers with numerous intercalated and exchangeable anions, enabling them to function as excellent 2D adsorbents and ion exchangers with greater specific surface area and controllable interlayer spacing. Chen *et al.* anchored Co single atoms in LDHs to activate PMS to produce surface-bonded ROS selectively and sustainably (Fig. 11f).[196] The PMS with a negative charge was confined in interlayers of LDHs with positive charge and activated by Co sites. The unique nanoconfined structure could conceivably enhance the longevity of surface-attached radical species and prevent their decomposition.

3D confined space has a rich pore structure and a large internal space, which can accommodate more single atoms and provide rich active sites. Moreover, in contrast to 1D and 2D counterparts, 3D nanoconfined spaces generally exert less stringent constraints on molecular size. The 3D connectivity of the pores enables the reactant molecules to approach the active sites from multiple directions, increasing the probability of the reaction. Employing mesoporous silicon spheres featuring surface nanopores as supports, Meng *et al.* engineered Co single-atom catalysts with tailored degrees of nanoconfinement through meticulous regulation of the nanopore structures (Fig. 11g–l).[197] Systematic investigations revealed that the nanoconfinement effect not only substantially augmented reactant enrichment and interfacial mass transfer efficiency but also instigated a transition in the catalytic reaction pathway, shifting from a $^1O_2$ dominated mechanism towards a direct electron transfer process. Consequently, this strategic design led to a remarkable enhancement in both the degradation efficiency of electron-rich pollutants and the utilization rate of PMS, underscoring the pivotal role of nanoconfinement in optimizing catalytic performance. Some nanoconfined spaces

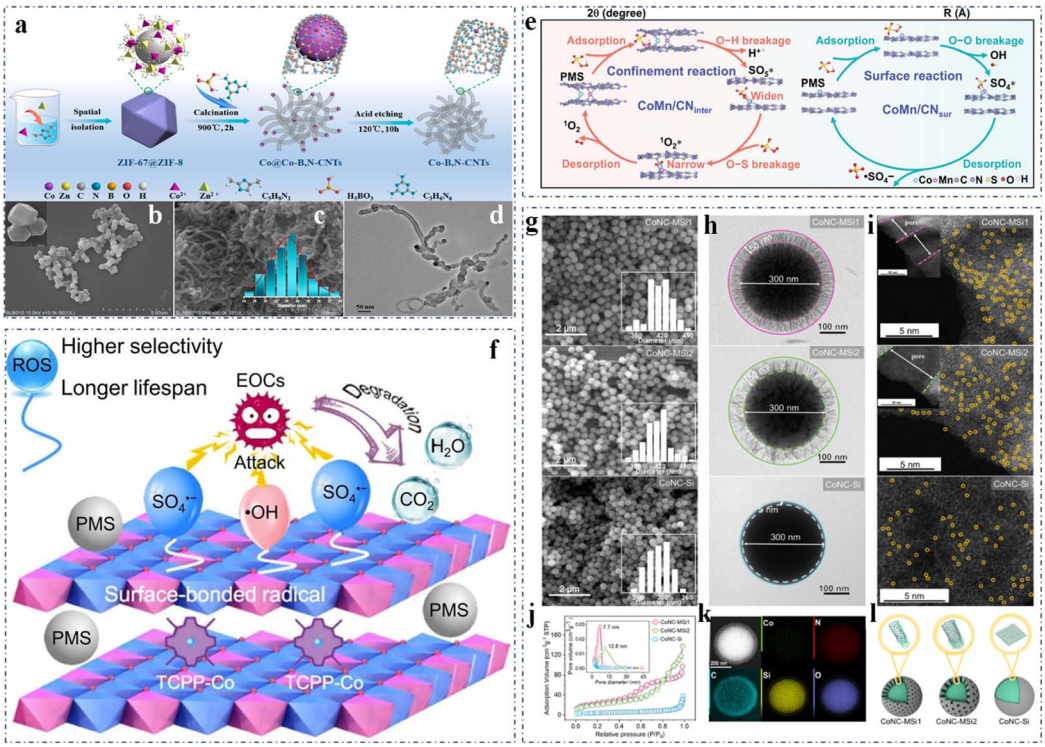

Fig. 11 (a) The synthesis strategy for Co–B, N-CNTs. (b) SEM image of ZIF-67@ZIF-8. (c) SEM and (d) TEM images of Co@Co–B, N-CNTs. Copyright 2023, Elsevier. (e) Possible photo-Fenton-like reaction under angstrom confinement (left) and surface (right) of CoMn/NC. Copyright 2025, Wiley-Advanced. (f) Schematic illustration of the degradation mechanism of contaminants in SA-Co-LDH. Copyright 2024, Elsevier. (g) SEM images and the particle size distribution, (h) TEM images, (i) AC-HAADF-STEM images, (j) EDS mapping, (k) N_2 adsorption–desorption isotherms and the pore size distribution of CoNC–MSi_1 catalyst. (l) Schematic diagram of the catalyst's spatial structure. Copyright 2024, Springer Nature.

go beyond traditional classification, encompassing surfaces, interfaces, or lattices, and exhibiting unique properties and behaviors. For example, the construction of surface nano-restricted structures can control the microenvironment around reactants and the catalyst, thereby ultimately influencing the reaction rate, selectivity and efficiency. Huang *et al.* reported a structure in which single-dispersed Fe atoms were loaded onto mesoporous nitrogen-doped carbon (FeSA–MNC), and used it as an effective PMS activator. Due to the excellent exposure of active sites and the surface confinement effect, the removal efficiency of pollutants has been greatly improved.[190] Interface confinement usually refers to nanoconfined effects induced by the interface between two materials that have a contact interface structure. Lattice nanoconfinement occurs when atoms, molecules, or clusters are embedded within the lattice framework of a catalyst.[186] The embedded species must be small to fit into the lattice, enabling this confinement to finely tune the atomic-level properties of the catalyst. However, it is noted that the application of interface and lattice confinement effects in regulating the microenvironment of SACs in Fenton-like reactions has not been widely reported up to now. Developing precise synthesis methods for accurately positioning and stably anchoring single atoms at interfaces and within lattices is crucial. This not only helps explore their excellent performance in Fenton-like systems but also reveals structure–activity relationships, guiding the design of efficient catalysts.

Overall, the confinement effect, as an effective regulatory strategy, demonstrates great potential in the regulation of the microenvironment of SACs. By constructing different types of confinement spaces, the electronic structure, coordination environment, and reaction microenvironment of single atoms can be precisely controlled, thereby enhancing the Fenton-like catalytic performance of SACs. Currently, research on the regulation of the microenvironment of SACs by the confinement effect has made significant progress in electrocatalysis, fuel cells and other energy catalysis systems, but still faces many challenges in environmental catalysis fields. For instance, the regulatory mechanisms of the confinement effect on the ROS generation pathway are still unclear. Using the confinement effect to drive the transformation of the radical and non-radical mechanism remains a major challenge that should be further explored in depth.

3.4 External field regulation

External field regulation, as an emerging strategy, provides a new approach for optimizing the microenvironment of SACs, which can significantly affect the catalytic activity, selectivity and stability of the catalyst. Theoretically, the electric field can change the distribution and structure of the electron cloud of

the catalyst, optimize the adsorption–desorption of reactants, and accelerate electron transfer. For example, Pan *et al.* reported that the hydrogen evolution performance of a Pt SAC could be enhanced by using external electric field polarization (Fig. 12a–k).[198] Specifically, the oriented external electric field could significantly modulate the electron distribution of single Co sites and the key reaction intermediates during electrocatalysis, thereby optimizing the reaction kinetics of the rate-determining step and enhancing the reaction performance. It is worth noting that there are very few studies on the influence of external electric field regulation on the Fenton-like activity of SACs. In Mu's report, the authors indicated that the cleavage of the O–H bond with high bond dissociation energy was the decisive step for the selective generation of Co(IV)=O species (Fig. 12l–p).[153] The coupling electron-proton transfer (CEPT) process could be utilized to achieve thermodynamically favorable O–H bond cleavage, and this process might be achieved by regulating the coordination configurations of SACs. Therefore, an asymmetrically coordinated Co SAC (CoB_1N_3) was fabricated in this work to induce a robust local electric field. This field promoted coupled electron-proton transfer, thermodynamically favoring O–H bond cleavage, which enabled O–O bond scission and efficient electron transfer for the selective generation of Co(IV)=O species.

The spin state regulation of SACs can be achieved by altering the electron spin distribution of the central metal atom at the

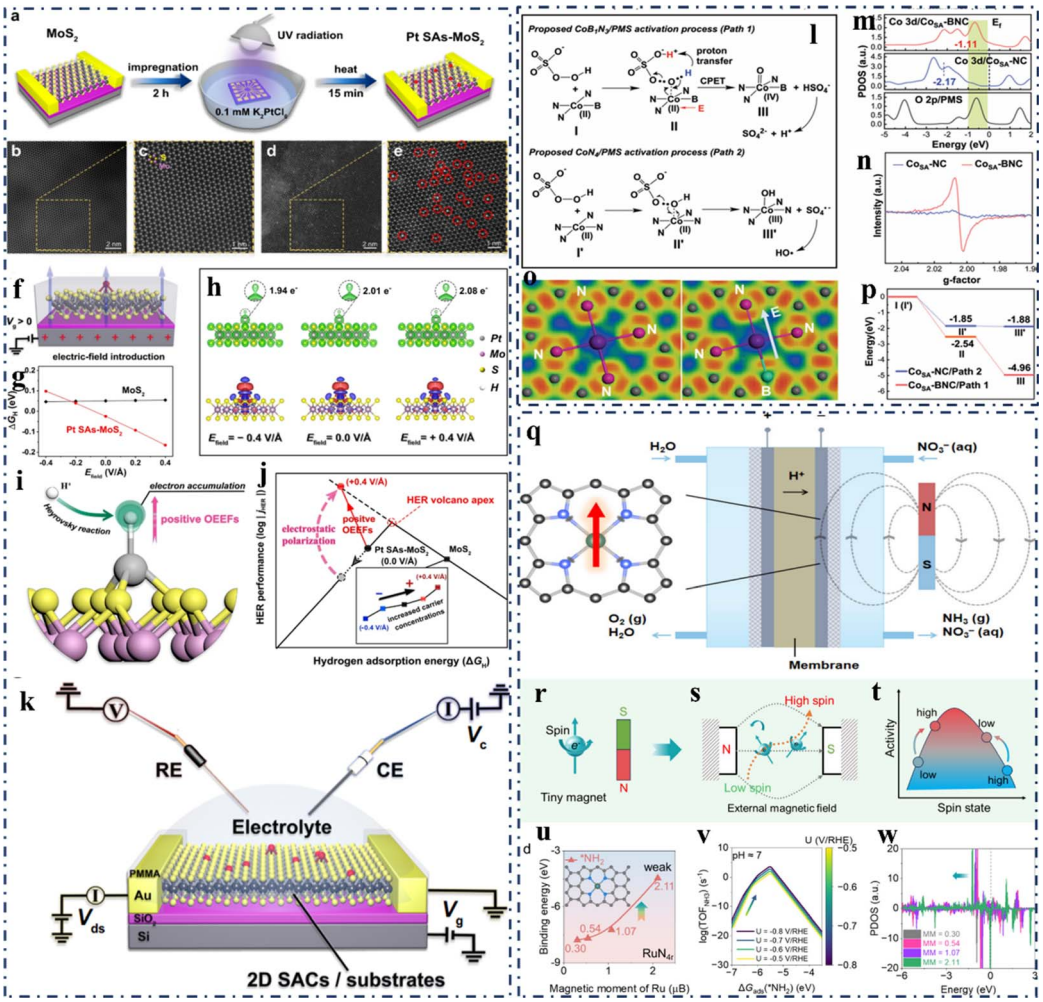

Fig. 12 (a) The preparation of Pt SAs–MoS_2 micro-device. HAADF-STEM images of (b) and (c) monolayer MoS_2 and (d) and (e) Pt SAs–MoS_2. (f) Schematic diagram of electric-field introduction into Pt SAs–MoS_2. (g) Hydrogen adsorption energy (ΔG_H) in 2H-MoS_2 and (M-top)–Pt SAs–MoS_2. (h) Charge analysis of (M-top)–Pt SAs–MoS_2. (i) The "onsite electrostatic polarization" mechanism on Pt SAs–MoS_2 for the HER. (j) The positive-OEEF-induced breakthrough at the HER volcano apex in Pt SAs–MoS_2. (k) An on-chip four-electrode microcell for electronic/electrochemical measurements. Copyright 2022, Springer Nature. (l) Proposed PMS activation pathways catalyzed by CoSA–BNC and CoSA–NC. (m) PDOS of Co 3d in CoB_1N_3, Co 3d in CoN_4 and absorbed O 2p in PMS. (n) Low-temperature EPR test of CoSA–NC and CoSA–BNC. (o) Electron localization function analysis of CoN_4 (left) and CoB_1N_3 (right). (p) Energy profiles of PMS activation by the two configurations. Copyright 2023, Springer Nature. (q) Mechanism of external magnetic field regulation to Ru–N–C. (r) Schematic of spinning electrons functioning as tiny magnets. (s) Polarized electron generation under an external magnetic field. (t) The correlation between the spin state of metal sites and their delivered activity. (u) *NH_2 binding energy on pyrrolic N supported single-atom Ru(v) derived pH-dependent activity volcano plot of electrochemical NO_3^- reduction. (w) PDOS of Ru at various magnetic moment levels. Copyright 2025, American Chemical Society.

active site (such as the conversion between low spin and high spin), optimizing the adsorption energy of the reaction substrates/intermediates, adjusting the reaction energy barrier, and regulating the product formation pathway, thereby significantly enhancing the activity, selectivity, and stability of the catalytic reaction. In You's work, the spin state of Ru single-atom catalysts (Ru–N–C) supported on nitrogen-doped carbon was regulated by an external magnetic field to optimize their catalytic performance in electrochemical nitrate reduction (NitRR) (Fig. 12q–w).[199] An external magnetic field induced the formation of a high-spin state in Ru SACs, which exhibited considerable NH_3 yield rate and a high faradaic efficiency. Theoretical calculations further showed that the elevated spin state of Ru shifts the density of states (DOS) away from the Fermi level, weakening the adsorption affinity for the $*NH_2$ intermediate.

Notably, current research on the regulatory mechanisms of external fields on the microenvironment of SACs remains limited. As compared with traditional directions such as coordination environment regulation, support regulation, and confinement effect modulation, research on the microenvironment regulation of SACs by external fields in the Fenton-like reaction is still in its infancy. This is because the early studies on SAC microenvironment regulation focus on "static regulation". These strategies can be achieved through conventional material synthesis methods, leading to the rapid accumulation of the relevant literature in recent years. In contrast, external field regulation is "dynamic regulation", which requires integrating the coupling mechanism between physical fields and catalytic systems, as well as interdisciplinary collaboration. In addition, the interaction between external fields and SACs faces many challenges during the reaction. Specifically, it is necessary to precisely control parameters such as field intensity, frequency, and action time. It is also required to track the dynamic changes in the coordination structures and electron density of single atoms. When analyzing the impact of catalysts on PMS decomposition, the interference of external fields on the decomposition performance of PMS should be eliminated, as these external fields themselves can also affect the decomposition of PMS. To fill the research gap, future studies should integrate advanced *in situ* characterization (*e.g.*, *in situ* XAFS, EPR, Raman) and computational methods (DFT, MD simulations) to clarify field–microenvironment interaction mechanisms, such as how fields modulate the electronic states of SACs or intermediate adsorption. Rationally designing SACs with tailored properties (*e.g.*, support conductivity, magnetic susceptibility) is also key to maximizing field effects. These efforts will deepen understanding of field–SAC interactions and lay a foundation for high-performance Fenton-like systems for wastewater treatment.

Micro-environment regulation	Structural Features	Impact on Fenton-like Activity	Correlation with ROS Generation Pathways
Coordination Environmental Engineering	➤**Coordination number (low coordination and high coordination)** ➤**Ligand type (introducing heteroatom ligands like O/N/S/P...)** ➤**Coordination geometry modification (Planar and axial)**	➢Expose more active sites, enhancing catalytic activity; ➢Strengthen the oxidation capacity of metal centers, accelerating substrate activation; ➢Optimize reactant adsorption energy, increasing reaction rate;	➢O-containing ligands: Radical pathway ($SO_4^{\bullet-}$ and •OH generation via PMS homolysis) ➢N/S/P-dominated ligands: Non-radical pathway ($^1O_2$, ETP) ➢Low/High-coordination : Enhanced non-radical pathway
Electron regulation mediated by supports/ ligands	➤**Support surface modification (defect sites, doping heteroatoms)** ➤**Strong metal-support interaction (SMSI) (regulate electron density)** ➤**Ligand electronic effect**	➢Optimized electron density promotes electron transfer between metal centers and substrates, accelerating reactions ➢Strong interactions stabilize highly active intermediates, extending catalytic lifespan	➢Carbon defects: Induce the formation of surface-bonded radicals ➢Vacancies (O/S): Radical pathway ($SO_4^{\bullet-}$ and •OH) ➢SMSI: High-valent metal species, ETP
Spatial confinement regulation	➤**Confinement size (mesoporous/microporous)** ➤**Dimension and structural characteristics (1D, 2D, 3D)** ➤**Optimization of active site spatial arrangement**	➢Enrich reactants increasing local reaction concentration; ➢Optimize the adsorption and activation ability of the reactant molecules; ➢High-density confinement increases the number of active sites per unit area;	➢Induce the formation of surface-bonded PMS* ➢Stabilization of high-valent metal species ➢Strengthens the non-radical electron transfer pathway
External field regulation	➤**Light field assistance** ➤**Electric field regulation (applying external voltage to adjust electron transfer direction)** ➤**Magnetic field assistance (enhancing mass transfer or electron spin regulation)**	➢Accelerate metal ion reduction (e.g., $Fe^{3+}\rightarrow Fe^{2+}$), alleviating active site deactivation ➢Drive electron transfer, improving reaction kinetic rates ➢Enhance reactant mass transfer, increasing catalytic activity	➢Light assistance: Strengthen radical pathway ➢Electric field: Non-radical pathway ➢Magnetic field: Non-radical pathway

Fig. 13 Correlations among active-center microenvironment structures, Fenton reactivity, and ROS generation pathways.

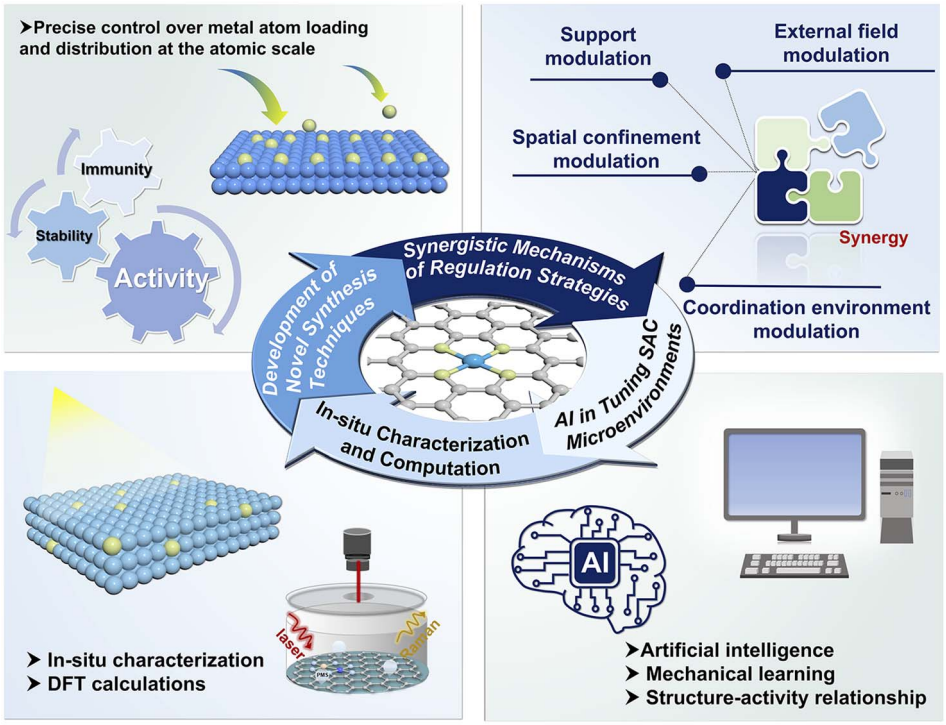

Fig. 14 Schematic illustration of future research challenges and opportunities.

4. Summary and perspectives

This review has systematically summarized and analyzed the applications of microenvironment regulation strategies for single-atom catalysts (SACs) in Fenton-like reactions. By modulating the coordination environment to change the type and number of ligands around the active centers, regulating the support effect to achieve support modification and the interaction between active sites and supports, tuning the electronic structure through means such as doping or external field effects, and controlling the spatial confinement to influence the local environment of the active centers, the performance of Fenton-like reactions has been enhanced, and the relevant mechanisms have been revealed. Taking the active centers of carbon-based SACs as examples, these microenvironment regulation strategies have achieved remarkable breakthroughs in enhancing the activity of Fenton-like reactions, optimizing reaction mechanisms, and improving selectivity. Meanwhile, these studies have preliminarily clarified the relationships between the microenvironment structures of different active centers and the activity and mechanisms of Fenton-like reactions, providing a theoretical basis for understanding the role of SACs in Fenton-like systems, as summarized in Fig. 13. Nevertheless, their practical implementation still faces numerous challenges that necessitate multi-dimensional exploration spanning synthesis methodologies, mechanistic investigations, and performance optimization. Future research endeavors should prioritize four critical aspects (Fig. 14).

4.1 Development of novel synthesis techniques

Development of more convenient, efficient, and environmentally friendly preparation methods for precise microenvironment regulation of SACs remains a key research focus. Current synthetic approaches for SACs often encounter issues such as low metal loading, uneven atomic dispersion, and complex preparation procedures, which hinder their large-scale applications. Exploring innovative synthesis techniques holds promise for achieving precise control over the microenvironment of SACs. For example, novel templating methods, represented by MOFs, have become a key technology to solve the contradiction between high loading and high dispersion of SACs through its unique structural design and chemical environment regulation. The ordered porous structure of MOFs provides a nanoscale "cage" for metal atoms, and the N, O and other heteroatoms in their ligands can firmly anchor the metal centers through coordination bonds, inhibiting atom agglomeration. The obtained SACs inherit the mesoporous structure of MOFs and have excellent mass transfer efficiency. *In situ* synthesis methods are employed during the formation of supports, where metal precursors simultaneously participate in the reaction and are *in situ* anchored to defect sites (such as oxygen vacancies and nitrogen defects), thus avoiding the migration and agglomeration of metal atoms in separate loading steps. Combined with nano-confined thermal pulse technology (NIS), *in situ* synthesis can achieve precise regulation of multi-metallic single atoms. The integration of cutting-edge techniques like atomic layer deposition (ALD) with chemical vapor deposition (CVD) strategies holds promise for achieving precise control over metal atom loading and distribution at the

atomic scale, thereby ensuring the consistency and stability of SACs. The ALD–CVD method is not a simple superposition of two technologies, but based on the collaboration of precise support construction and atomic-level load regulation. High-temperature CVD prepares supports with high specific surface area and multi-level pore structure. ALD then uses its "self-limiting surface reaction" to alternately introduce metal precursors and deposit single metal atoms layer by layer on support defects or active sites. Bio-templating is a novel green synthesis strategy that uses natural biomolecules as templates to prepare SACs. Biomolecules contain abundant N, O, S, P and other heteroatoms, which act as anchor sites to strongly coordinate with metal atoms, inhibiting their agglomeration and precisely regulating their electronic state. At present, the synthesis of SACs by biological template methods is still in the transition stage from laboratory research to pilot production. However, its advantages in terms of greenness, precision and low cost have demonstrated clear development potential. Future advances may take SACs from lab research to industrial use. This will support large-scale SAC applications in green energy, high-end chemicals and biomedicine. It will also promote sustainable catalysis in industry, contributing to the realization of the "dual carbon" goals.

Additionally, based on the aforementioned advanced synthetic approaches, it is imperative to conduct systematic studies on the stability, catalytic activity, and anti-interference capabilities of SACs in real-world scenarios. Such research will be critical for extending their practical use in treating complex wastewater and purifying industrial wastes. Optimizing microenvironment regulation strategies to enhance the adaptability of SACs to complex practical systems will lay a solid foundation for the widespread implementation of Fenton-like reactions in environmental governance.

4.2 Synergistic mechanisms of different regulation strategies

Presently, research on microenvironment regulation of SACs has primarily focused on individual strategies, such as support modification or ligand engineering, still facing trade-offs between activity, selectivity, and stability. Future studies can delve into the synergistic effects which can effectively integrate the advantages of ligand engineering (precise coordination control, optimized electronic state), defect engineering (increased anchoring sites, promoted substrate adsorption), and support modification (enhanced SMSI, improved conductivity), realizing "1 + 1 > 2" performance improvements. For example, combining the electronic modulation capabilities of supports with the steric hindrance effects of ligands can enable dual optimization of the electronic structure and reaction selectivity of metal active centers, enhancing the generation capacity of active species, inhibiting structural deformation by strengthening the metal–support interaction, and achieving dual regulation of the metal centers.

In addition, confining single atoms within porous support structures (confinement regulation) helps concentrate PMS and reaction intermediates in the local microspace, alleviating mass transfer limitations. Meanwhile, adjusting the coordination configuration of single atoms *via* surface ligand modification (coordination environment regulation) optimizes their electronic state, reducing the energy barrier for PMS activation. This synergy not only enhances the generation efficiency of ROS compared to standalone confinement regulation but also suppresses single-atom aggregation. In turn, it maintains long-term catalytic activity, which is achieved through the combined effects of spatial constraints from pores and chemical anchoring from ligands. Finally, establishing multi-scale models that integrate experimental data with theoretical calculations to quantitatively analyze the impacts of synergistic regulation on the kinetics and thermodynamics of Fenton-like reactions will provide a theoretical foundation for the rational design of high-performance catalysts. Moreover, developing such synergistic strategies is not only a research focus but an inevitable requirement to break through current performance bottlenecks for SACs to move from laboratory research to industrial applications.

4.3 *In situ* characterization and computation for reaction mechanistic insights

During Fenton-like reactions, the short lifetimes of reactive intermediates (*e.g.*, $^{\bullet}OH$, $SO_4^{\bullet-}$, $^1O_2$, high-valent metal species) and the complexity of parallel reaction pathways (radical *vs.* non-radical mechanisms) pose significant challenges for conventional characterization techniques. The advancement of *in situ* characterization technologies, coupled with quantum chemical calculations, is revolutionizing our ability to decode dynamic reaction mechanisms and guide rational catalyst design. For instance, *in situ* Raman spectroscopy has been applied to identify the surface-bound intermediates during PMS activation by SACs. Time-resolved Raman spectra captured a transient catalyst/PMS* intermediate during the reaction, providing direct evidence for the non-radical pathway, such as high-valent metal–oxo species and electron transfer processes. Similarly, *in situ* X-ray absorption spectroscopy (XAS) has been used to monitor metal coordination changes in M–N–C SACs during PMS activation. Extended X-ray absorption fine structure (EXAFS) analysis revealed a dynamic change of M–N bond lengths under reaction conditions, corresponding to the formation of reactive intermediates, which can be further confirmed by X-ray absorption near-edge structure (XANES) shifts in the K-edge of the metals. Coupling *in situ* experimental techniques with quantum chemical calculations, such as density functional theory (DFT), provides precise guidance for catalyst optimization by clarifying dynamic mechanisms. Specifically, experiments can identify key intermediates and track structural changes, while calculations are able to quantify energy barriers and determine rate-limiting steps (such as O–O bond cleavage during PMS activation). This collaborative approach reveals how microenvironmental characteristics affect reaction activity, laying the foundation for targeted design. For instance, adjusting metal–ligand configurations can reduce activation energy barriers or stabilize active

intermediates, thereby improving catalytic efficiency and selectivity in Fenton-like reactions.

4.4 AI in tuning SAC microenvironments for enhanced performance

Artificial intelligence (AI) is an emerging powerful tool in the field of materials science research, capable of analyzing vast experimental datasets to predict the relationships between the performance and structural parameters of SACs. Machine learning algorithms can be employed to establish quantitative models that link microenvironmental parameters (*e.g.*, support properties, ligand structures) to catalytic activity, thereby accelerating the design and preparation of novel catalysts. AI enables targeted solutions to key challenges in SAC microenvironment regulation and performance optimization. For example, we can employ machine learning models to simulate the impact of ligand electronegativity, support defect density, and metal coordination number on PMS activation efficiency. The model can achieve a prediction accuracy for ROS generation ratios, enabling rapid screening of optimal M–N configurations for selective pollutant degradation. Moreover, an AI system that combines DFT calculations is expected to be used for exploring the regulation of the microenvironment of PMS-activated SACs and the optimization of their performance. Furthermore, AI-assisted high-throughput experimental platforms can facilitate rapid catalyst synthesis, significantly shorten the research and development cycle and promote the translation of SACs from laboratory-scale demonstrations to practical applications. AI-based *in situ* monitoring systems can be utilized to predict the relationship between the synthesis conditions and the final structure of the catalyst. *In situ* tracking is conducted during the synthesis process of single-atom catalysts to observe the structural evolution of single-atom sites. The synthesis parameters are adjusted in real time based on the coordination state, further expanding the application scenarios of synthesis methods.

Author contributions

Conceptualization: Na Wang and Jie Yang; writing – original draft: Na Wang and Jie Yang; writing – review & editing: Ziqiu Ren and Qun Xu; visualization: Na Wang, Sixun Li and Jie Yang; supervision: Na Wang and Ziqiu Ren.

Conflicts of interest

There are no conflicts to declare.

Data availability

No primary research results, software, or code have been included, and no new data were generated or analyzed as part of this review.

Acknowledgements

This work has received financial support from the National Natural Science Foundation of China (No. 22105178, 52103237) and Foundation of Henan Educational Committee (35220105).

Notes and references

1 P. Babuji, S. Thirumalaisamy, K. Duraisamy and G. Periyasamy, *Water*, 2023, **15**, 2532–2547.
2 R. Xiao, Z. Luo, Z. Wei, S. Luo, R. Spinney, W. Yang and D. D. Dionysiou, *Curr. Opin. Chem. Eng.*, 2018, **19**, 51–58.
3 P. Hu and M. Long, *Appl. Catal., B*, 2016, **181**, 103–117.
4 E. Brillas and S. Garcia-Segura, *Sep. Purif. Technol.*, 2020, **237**, 116337.
5 I. A. Ike, K. G. Linden, J. D. Orbell and M. Duke, *Chem. Eng. J.*, 2018, **338**, 651–669.
6 L. Xu and J. Wang, *Environ. Sci. Technol.*, 2012, **46**, 10145–10153.
7 B. Gao, S. Zhu, J. Gu, Y. Liu, X. Yi and H. Zhou, *J. Hazard. Mater.*, 2022, **431**, 128549.
8 X. Duan, H. Sun, Z. Shao and S. Wang, *Appl. Catal., B*, 2018, **224**, 973–982.
9 W. Ren, C. Cheng, P. Shao, X. Luo, H. Zhang, S. Wang and X. Duan, *Environ. Sci. Technol.*, 2022, **56**, 78–97.
10 X. Duan, H. Sun and S. Wang, *Acc. Chem. Res.*, 2018, **51**, 678–687.
11 J. Lee, U. von Gunten and J. H. Kim, *Environ. Sci. Technol.*, 2020, **54**, 3064–3081.
12 Q. Fang, H. Yang, S. Ye, P. Zhang, M. Dai, X. Hu, Y. Gu and X. Tan, *Water Res.*, 2023, **245**, 120614.
13 F. Ghanbari and M. Moradi, *Chem. Eng. J.*, 2017, **310**, 41–62.
14 J. Wang and S. Wang, *Chem. Eng. J.*, 2018, **334**, 1502–1517.
15 W.-D. Oh, Z. Dong and T.-T. Lim, *Appl. Catal., B*, 2016, **194**, 169–201.
16 M. Kohantorabi, G. Moussavi and S. Giannakis, *Chem. Eng. J.*, 2021, **411**, 127957.
17 X. Chen, W.-D. Oh and T.-T. Lim, *Chem. Eng. J.*, 2018, **354**, 941–976.
18 S. Wu, H. Liu, C. Yang, X. Li, Y. Lin, K. Yin, J. Sun, Q. Teng, C. Du and Y. Zhong, *Chem. Eng. J.*, 2020, **392**, 123683.
19 J. Guo, B. Gao, Q. Li, S. Wang, Y. Shang, X. Duan and X. Xu, *Adv. Mater.*, 2024, **36**, e2403965.
20 P. Yang, Z. Cao, Y. Long, D. Liu, W. Huang, S. Zhan and M. Li, *ACS Catal.*, 2023, **13**, 12414–12424.
21 Y. Gao, T. Wu, C. Yang, C. Ma, Z. Zhao, Z. Wu, S. Cao, W. Geng, Y. Wang, Y. Yao, Y. Zhang and C. Cheng, *Angew Chem. Int. Ed. Engl.*, 2021, **60**, 22513–22521.
22 Y. Gao, B. Liu and D. Wang, *Adv. Mater.*, 2023, **35**, e2209654.
23 S. Li, Y. Zhang, J. Zhou and S. Qiao, *Small*, 2025, **21**, 2411230.
24 L. Li, X. Niu, D. Zhang, X. Ye, Z. Zhang, C. Wang, L. Ding, Y. Zhang, B. Li, X. Su, X. He, Y. Hu, D. Zhao, D. Chen and Y. Lin, *Appl. Catal., B*, 2025, **378**, 125585.
25 Z. Qi, Y. Zhou, R. Guan, Y. Fu and J. B. Baek, *Adv. Mater.*, 2023, **35**, 2210575.

26 W. Li, Z. Guo, J. Yang, Y. Li, X. Sun, H. He, S. Li and J. Zhang, *Electrochem. Energy Rev.*, 2022, **5**, 9.
27 Y. Zhang, J. Yang, R. Ge, J. Zhang, J. M. Cairney, Y. Li, M. Zhu, S. Li and W. Li, *Coord. Chem. Rev.*, 2022, **461**, 214493.
28 G. Li, J. Zhang, Z. Wu, H. Li, Y. Song and S. Zhang, *Mater. Today*, 2025, **85**, 141–170.
29 S. Ma, W. Han, W. Han, F. Dong and Z. Tang, *J. Mater. Chem. A*, 2023, **11**, 3315–3363.
30 W. Zhang, S. Zhang, C. Meng and Z. Zhang, *Appl. Catal., B*, 2023, **322**, 122098.
31 T. Liu, S. Xiao, N. Li, J. Chen, X. Zhou, Y. Qian, C. H. Huang and Y. Zhang, *Nat. Commun.*, 2023, **14**, 2881.
32 B. Han, Y. Luo, Y. Lin, B. Weng, D. Xia, Y. Zhou, C. Guan, Z. Wang, X. Wei and J. Jiang, *Chem. Eng. J.*, 2022, **447**, 137551.
33 L. Li, B. Huang, X. Tang, Y. Hong, W. Zhai, T. Hu, K. Yuan and Y. Chen, *Adv. Funct. Mater.*, 2021, **31**, 2103857.
34 F. Liu, Y. Ren, J. Duan, P. Deng, J. Lu, H. Ge, X. Liu, Q. Xia, H. Qi, N. Yang and Y. Qin, *Chem. Eng. J.*, 2023, **454**, 140382.
35 C. Yang, S. Shang, Y. Wang, P. Wang, L. Sun and X.-y. Li, *Chem. Eng. J.*, 2025, **514**, 163255.
36 G. Zhou, S. Zhao, T. Wang, S.-Z. Yang, B. Johannessen, H. Chen, C. Liu, Y. Ye, Y. Wu, Y. Peng, C. Liu, S. P. Jiang, Q. Zhang and Y. Cui, *Nano Lett.*, 2020, **20**, 1252–1261.
37 Q. Shao, L. Xu, D. Guo, Y. Su and J. Chen, *J. Mater. Chem. A*, 2020, **8**, 23772–23783.
38 W. Tan, S. Xie, D. Le, W. Diao, M. Wang, K.-B. Low, D. Austin, S. Hong, F. Gao, L. Dong, L. Ma, S. N. Ehrlich, T. S. Rahman and F. Liu, *Nat. Commun.*, 2022, **13**, 7070.
39 Z. Wang, S. Xie, Y. Feng, P. Ma, K. Zheng, E. Duan, Y. Liu, H. Dai and J. Deng, *Appl. Catal., B*, 2021, **298**, 120612.
40 C. Yang, S. Shang, Y. Wang, P. Wang, L. Sun and X.-y. Li, *Chem. Eng. J.*, 2025, **514**, 163255.
41 Z. Li, Y. Yang, C. Zhang, W. Fan, G. Li, J. Fang and L. Lu, *Chem Catal.*, 2024, **4**, 100902.
42 B. Liang, S. Guo, Y. Zhao, I. U. Khan, X. Zhang, K. Li and C. Lv, *J. Power Sources*, 2020, **450**, 227683.
43 Y. Gao, C. Yang, M. Zhou, C. He, S. Cao, Y. Long, S. Li, Y. Lin, P. Zhu and C. Cheng, *Small*, 2020, **16**, e2005060.
44 X. Li, X. Huang, S. Xi, S. Miao, J. Ding, W. Cai, S. Liu, X. Yang, H. Yang, J. Gao, J. Wang, Y. Huang, T. Zhang and B. Liu, *J. Am. Chem. Soc.*, 2018, **140**, 12469–12475.
45 W. Qu, C. Chen, Z. Tang, H. Wen, L. Hu, D. Xia, S. Tian, H. Zhao, C. He and D. Shu, *Coord. Chem. Rev.*, 2023, **474**, 214855.
46 H. Liu, W. Xiong, C. Zhou, C. Lai, L. Li, G. Wang, X. Huo, G. Zeng and M. Cheng, *Coord. Chem. Rev.*, 2025, **529**, 216468.
47 N. Daelman, M. Capdevila-Cortada and N. Lopez, *Nat. Mater.*, 2019, **18**, 1215–1221.
48 L. He, C. Guan, D. A. Bulushev and Q. Xiang, *Small*, 2024, 2410976.
49 R. Lang, X. Du, Y. Huang, X. Jiang, Q. Zhang, Y. Guo, K. Liu, B. Qiao, A. Wang and T. Zhang, *Chem. Rev.*, 2020, **120**, 11986–12043.
50 J.-C. Li, D.-M. Tang, P.-X. Hou, G.-X. Li, M. Cheng, C. Liu and H.-M. Cheng, *MRS Commun.*, 2018, **8**, 1158–1166.
51 Z. Wu, Z. Xiong, B. Huang, G. Yao, S. Zhan and B. Lai, *Nat. Commun.*, 2024, **15**, 7775.
52 V. Giulimondi, S. Mitchell and J. Perez-Ramirez, *ACS Catal.*, 2023, **13**, 2981–2997.
53 X. Liu, Y. Liu, W. Yang, X. Feng and B. Wang, *Chem*, 2022, **28**, e202201471.
54 H. Zhao, X. Xu, W. Cui, L. Geng, X. Peng, J. Yang, X. Shao and Y. Liu, *Adv. Mater.*, 2025, e2503217.
55 W. Ma, X. Ren, J. Li, S. Wang, X. Wei, N. Wang and Y. Du, *Small*, 2024, **20**, e2308957.
56 W.-Y. Huang, G.-Q. Wang, W.-H. Li, T.-T. Li, G.-J. Ji, S.-C. Ren, M. Jiang, L. Yan, H.-T. Tang, Y.-M. Pan and Y.-J. Ding, *Chem*, 2020, **6**, 2300–2313.
57 S. Xin, L. Ni, P. Zhang, H. Tan, M. Song, T. Li, Y. Gao and C. Hu, *Adv. Sci.*, 2023, **10**, 2304088.
58 B. Liu, X. Huang, W. Guo, H. Wang, C. Yang, J. Gao, F. He, L. Liang and Z. Wang, *Chem. Eng. J.*, 2024, **499**, 156042.
59 J. Li, Y. Zou, Z. Li, S. Fu, Y. Lu, S. Li, X. Zhu and T. Zhang, *ACS Appl. Mater. Interfaces*, 2022, **14**, 37865–37877.
60 Z. Zeng, J. Xu, Y. Zhao, J. Li, C. Du, Y. Sun and H. Xiong, *ChemCatChem*, 2024, **16**, e202400091.
61 C. Bellouard, S. Kim, J. Ghanbaja, R. Wojcieszak, N. Canilho and A. Pasc, *J. Phys. Chem. C*, 2024, **128**, 8449–8457.
62 Y. Gao, X. Duan, B. Li, Q. Jia, Y. Li, X. Fan, F. Zhang, G. Zhang, S. Wang and W. Peng, *J. Mater. Chem. A*, 2021, **9**, 14793–14805.
63 J. Song, N. Hou, X. Liu, M. Antonietti, Y. Wang and Y. Mu, *Appl. Catal., B*, 2023, **325**, 122368.
64 X. Li, M. Liu, L. Wen, R. Li, Y. Liu, S. Yang, D. Ding, Y. Chen, R. Chen and S. Xu, *Environ. Sci. Technol.*, 2025, **59**, 13458–13469.
65 J. Cui, L. Li, S. Shao, J. Gao, K. Wang, Z. Yang, S. Zeng, C. Diao, Y. Zhao and C. Hu, *ACS Catal.*, 2022, **12**, 14954–14963.
66 Y. Li, T. Yang, S. Qiu, W. Lin, J. Yan, S. Fan and Q. Zhou, *Chem. Eng. J.*, 2020, **389**, 124382.
67 Y. Lin, W. Qin, Y. Lu, M. Ren, P. Gao, F. Xiao and S. Yang, *Environ. Sci.: Nano*, 2023, **10**, 1284–1296.
68 T. Chen, G. Zhang, H. Sun, Y. Hua, S. Yang, D. Zhou, H. Di, Y. Xiong, S. Hou, H. Xu and L. Zhang, *Nat. Commun.*, 2025, **16**, 2402.
69 Y. Shen, M. Yang, C. Zhu, H. Zhang, R. Liu, J. Wang, Q. Fang, S. Song and B. Chen, *ACS ES&T Eng.*, 2024, **4**, 2839–2851.
70 J. Yang, D. Zeng, Q. Zhang, R. Cui, M. Hassan, L. Dong, J. Li and Y. He, *Appl. Catal., B*, 2020, **279**, 119363.
71 L. Zhang, Y. Sun, R. Ge, W. Zhou, Z. Ao and J. Wang, *Appl. Catal., B*, 2023, **339**, 123130.
72 K. Qian, H. Chen, W. Li, Z. Ao, Y. N. Wu and X. Guan, *Environ. Sci. Technol.*, 2021, **55**, 7034–7043.
73 B. Zhang, X. Li, K. Akiyama, P. A. Bingham and S. Kubuki, *Environ. Sci. Technol.*, 2022, **56**, 1321–1330.
74 K. Yin, L. Peng, D. Chen, S. Liu, Y. Zhang, B. Gao, K. Fu, Y. Shang and X. Xu, *Appl. Catal., B*, 2023, **336**, 122951.

75 J. Wang, S. Chen, B. Li, W. Ren, Y. Zhu, X. Liu, Z. Liu, F. Xia, M. Cheng and J. Zou, *Sep. Purif. Technol.*, 2025, **375**, 133785.
76 M. Yang, R. Wu, S. Cao, Y. Li, S. Huo, W. Wang, Z. Hu and X. Xu, *Chem. Eng. J.*, 2023, **451**, 138606.
77 X. Mi, P. Wang, S. Xu, L. Su, H. Zhong, H. Wang, Y. Li and S. Zhan, *Angew Chem. Int. Ed. Engl.*, 2021, **60**, 4588–4593.
78 Y. Xiong, H. Li, C. Liu, L. Zheng, C. Liu, J. O. Wang, S. Liu, Y. Han, L. Gu, J. Qian and D. Wang, *Adv. Mater.*, 2022, **34**, e2110653.
79 J. Zhang, S. Qu, B. Li, X. Li and L. Lin, *Chem. Eng. J.*, 2023, **468**, 143593.
80 W. Zhang, M. Li, J. Luo, G. Zhang, L. Lin, F. Sun, M. Li, Z. Dong and X.-y. Li, *Chem. Eng. J.*, 2023, **474**, 145377.
81 P. Cui, Q. Yang, C. Liu, Y. Wang, G. Fang, D. D. Dionysiou, T. Wu, Y. Zhou, J. Ren, H. Hou and Y. Wang, *ACS ES&T Eng.*, 2021, **1**, 1460–1469.
82 T. Sun, Y. Liu, J. Li, Y. Zhang, B. Zhao, M. Li, C. Zhang, M. Huo, J. Jiang and S. Dong, *Appl. Catal., B*, 2025, **371**, 125283.
83 Y. Long, Z. Cao, W. Wu, W. Liu, P. Yang, X. Zhan, R. Chen, D. Liu and W. Huang, *Appl. Catal., B*, 2024, **344**, 123643.
84 Y. Fan, D. Kong, F. Wang, Z. Sun, J. Yao, M. Chu, Y. Zhou, C. H. Tung and Y. Wang, *Small*, 2025, **21**, e2409240.
85 Z. Li, J. Lu, T. Zhang, Y. Liu, R. Pan, Q. Fu, X. Liu, S. Mao and B. Xu, *J. Colloid Interface Sci.*, 2024, **674**, 279–288.
86 T. Chen, G. Zhang, H. Sun, Y. Hua, S. Yang, D. Zhou, H. Di, Y. Xiong, S. Hou, H. Xu and L. Zhang, *Nat. Commun.*, 2025, **16**, 2402.
87 X. Zhou, M.-K. Ke, G.-X. Huang, C. Chen, W. Chen, K. Liang, Y. Qu, J. Yang, Y. Wang, F. Li, H.-Q. Yu and Y. Wu, *Proc. Natl. Acad. Sci. U. S. A.*, 2022, **119**, e2119492119.
88 Z. Yang, X. Yang, W. Zhang, J. Ai and D. Wang, *ACS ES&T Water*, 2024, **4**, 3297–3308.
89 H. Dai, Z. Zhao, K. Wang, F. Meng, D. Lin, W. Zhou, D. Chen, M. Zhang and D. Yang, *J. Hazard. Mater.*, 2024, **465**, 133399.
90 Z. Wu, B. Huang, X. Wang, C. S. He, Y. Liu, Y. Du, W. Liu, Z. Xiong and B. Lai, *Environ. Sci. Technol.*, 2023, **57**, 14046–14057.
91 S. Zhang, B. Sun, K. Liao, X. Wang, Z. Chen, J. Wang, W. Hu and X. Han, *Adv. Funct. Mater.*, 2025, 202425640.
92 Y. Zou, S. Fu, Z. Xu, X. Zhou, J. Li, Y. Zhang, Y. Lu, S. Li and T. Zhang, *Chem. Eng. J.*, 2025, **505**, 2425640.
93 K. Yin, R. Wu, Y. Shang, D. Chen, Z. Wu, X. Wang, B. Gao and X. Xu, *Appl. Catal., B*, 2023, **329**, 122558.
94 F. Xu, C. Lai, M. Zhang, B. Li, L. Li, S. Liu, D. Ma, X. Zhou, H. Yan, X. Huo, B. Wang, H. Yi, L. Qin and L. Tang, *Appl. Catal., B*, 2023, **339**, 123075.
95 X. Liang, D. Wang, Z. Zhao, T. Li, Y. Gao and C. Hu, *Adv. Funct. Mater.*, 2022, **32**, 2203001.
96 Y. Lin, Y. Wang, Z. Weng, Y. Zhou, S. Liu, X. Ou, X. Xu, Y. Cai, J. Jiang, B. Han and Z. Yang, *Nat. Commun.*, 2024, **15**, 10032.
97 Q. Du, C. Zhu, C. Yue, F. Cun, Z. Du, F. Liu and A. Li, *Appl. Catal., B*, 2024, **343**, 123570.
98 Q.-Y. Wu, Z.-W. Yang, Z.-W. Wang and W.-L. Wang, *Proc. Natl. Acad. Sci. U. S. A.*, 2023, **120**, e2219923120.
99 L. Zhang, N. Jin, Y. Yang, X. Y. Miao, H. Wang, J. Luo and L. Han, *Nano-Micro Lett.*, 2023, **15**, 228.
100 X. Zhang, C. Li, X. Wang, S. Yang, Y. Tan, F. Yuan, S. Zheng, D. D. Dionysiou and Z. Sun, *Small*, 2022, **18**, e2204793.
101 S. Jin, W. Tan, X. Tang, M. Li, X. Yu, H. Zhang, S. Song and T. Zeng, *Small*, 2024, **20**, e2405012.
102 Q. Jin, C. Wang, Y. Guo, Y. Xiao, X. Tan, J. Chen, W. He, Y. Li, H. Cui and C. Wang, *Adv. Sci.*, 2023, **10**, e2302152.
103 X. Wang, Z. Y. Yi, Y. Q. Wang and D. Wang, *Angew Chem. Int. Ed. Engl.*, 2025, **64**, e202413673.
104 K. Miao, J. Qin, S. Lai, M. Luo, A. Kuchkaev, D. Yakhvarov and X. Kang, *Adv. Funct. Mater.*, 2024, **35**, 2419989.
105 Y. Chen, H. Zhang, Y. Li, W.-W. Li, G.-P. Sheng and Y. Wang, *ACS Nano*, 2025, **19**, 14187–14199.
106 Y. Fan, M. Chu, H. Li, Z. Sun, D. Kong, J. Yao, G. Wang, Y. Wang and H.-Y. Zhu, *Small*, 2024, **20**, 2403804.
107 S. Jin, W. Tan, X. Tang, M. Li, X. Yu, H. Zhang, S. Song and T. Zeng, *Small*, 2024, **20**, 2405012.
108 Y. Bai, G. Zhang, M. Liu, S. Hou, S. Zheng, S. Yang, C. Zhu and H. Xu, *Appl. Catal., B*, 2025, **374**, 125378.
109 H. Fu, J. Wei, G. Chen, M. Xu, J. Liu, J. Zhang, K. Li, Q. Xu, Y. Zou, W.-x. Zhang, S. Xi, X. Chen, S. Li and L. Ling, *Appl. Catal., B*, 2023, **321**, 122012.
110 C. Gu, Y. Zhang, P. He, M. Gan, J. Zhu and H. Yin, *J. Hazard. Mater.*, 2024, **472**, 134515.
111 Y. Shen, Y. Pan, C. Zhu, H. Zhang, J. Wang, R. Liu, Q. Fang, S. Song and B. Chen, *Small*, 2024, **20**, e2406319.
112 S. Ren, Y. Wang, L. Shi, X. Xu, S. Zhong, K. Hu, H. Zhou, Z. S. Zhu, P. Zhou, W. Tian, J. Zuo, J. Yi, X. Guan, X. Duan and S. Wang, *Adv. Mater.*, 2025, **37**, e2415339.
113 Z. Zhu, Y. Wang, P. Wang, S. Zhong, K. Hu, S. Ren, J. P. Vongsvivut, H. Sun, X. Duan and S. Wang, *Nat. Water*, 2025, 1–11.
114 H. Shi, H. Zhang, T. Wang and S. Chen, *J. Hazard. Mater.*, 2025, **488**, 137483.
115 X. Li, J. Hu, Y. Deng, T. Li, Z.-Q. Liu and Z. Wang, *Appl. Catal., B*, 2023, **324**, 122243.
116 Z. Wang, E. Almatrafi, H. Wang, H. Qin, W. Wang, L. Du, S. Chen, G. Zeng and P. Xu, *Angew Chem. Int. Ed. Engl.*, 2022, **61**, e202202338.
117 L. Qin, J. Meng, G. Yang, Y. Pan, X. Gao, Y. Yang and Y. Guo, *Appl. Catal., B*, 2024, **345**, 123695.
118 Y. Zhao, B. Ma, X. Liu, N. Li, Y. Li, X. Fan and W. Peng, *Carbon*, 2023, **214**, 118371.
119 H. Meng, J. Zhou, Y. Zhang, J. Cui, Y. Chen, W. Zhong, Y. Chen and C. Q. Jia, *Appl. Catal., B*, 2025, **366**, 125038.
120 M. Fan, J. Cui, J. Wu, R. Vajtai, D. Sun and P. M. Ajayan, *Small*, 2020, **16**, 1906782.
121 N. Chen, Y. Zeng, T. Li, P. Cui, D. D. Dionysiou, X. Wang, C. Liu, G. Fang, C. Ding, Y. Zhao, J. Gao, Y. Wang and D. Zhou, *J. Hazard. Mater.*, 2023, **454**, 131480.
122 J. Liu, J. Zhu, H. Xu and D. Cheng, *ACS Catal.*, 2024, **14**, 6952–6964.
123 L. Su, P. Wang, X. Ma, J. Wang and S. Zhan, *Angew Chem. Int. Ed. Engl.*, 2021, **60**, 21261–21266.

124 F. Chen, Y. J. Sun, X. T. Huang, C. W. Bai, Z. Q. Zhang, P. J. Duan, X. J. Chen, Q. Yang and H. Q. Yu, *Proc. Natl. Acad. Sci. U. S. A.*, 2024, **121**, e2314396121.
125 C. Chen, Y. Shang, S. Shao, W. Wang, J. Zhu, Y. Gao, L. Chen and F. Wang, *J. Mater. Chem. A*, 2024, **12**, 25896–25908.
126 X. L. Wu, S. Liu, Y. Li, M. Yan, H. Lin, J. Chen, S. Liu, S. Wang and X. Duan, *Angew Chem. Int. Ed. Engl.*, 2023, **62**, e202305639.
127 J. Qiu, D. Wang, Y. Chang, Q. Feng, Z. Liu, M. Pang, D. Meng, Y. Feng and C. Fan, *Chem. Eng. J.*, 2024, **479**, 147841.
128 S. Wei, Y. Sun, Y. Z. Qiu, A. Li, C. Y. Chiang, H. Xiao, J. Qian and Y. Li, *Nat. Commun.*, 2023, **14**, 7549.
129 P. Cui, Q. Yang, C. Liu, Y. Wang, G. Fang, D. D. Dionysiou, T. Wu, Y. Zhou, J. Ren and H. Hou, *ACS ES&T Eng.*, 2021, **1**, 1460–1469.
130 J. Pei, H. Shang, J. Mao, Z. Chen, R. Sui, X. Zhang, D. Zhou, Y. Wang, F. Zhang, W. Zhu, T. Wang, W. Chen and Z. Zhuang, *Nat. Commun.*, 2024, **15**, 416.
131 L. S. Zhang, X. H. Jiang, Z. A. Zhong, L. Tian, Q. Sun, Y. T. Cui, X. Lu, J. P. Zou and S. L. Luo, *Angew Chem. Int. Ed. Engl.*, 2021, **60**, 21751–21755.
132 J. Wang, B. Li, Y. Li, X. Fan, F. Zhang, G. Zhang and W. Peng, *Adv. Sci.*, 2021, **8**, e2101824.
133 H. Zhong, J. Wang, B. Zhang, Y. Liu, Z. Gong, X. Xiao, J. Yu, Y. Hou, Y. Tao, H. Yang, Q. Fu, J. Zheng, P. Wang and G. Ouyang, *Adv. Funct. Mater.*, 2025, 2501208.
134 Y. Li, J. Wei, N. Cui, J. Li, W. Ji, L. Wang, J. Huo, W. Yan, X. Zhang, Y. Zhao and J. Li, *Appl. Catal., B*, 2024, **358**, 124385.
135 B. Huang, X. Ren, J. Zhao, Z. Wu, X. Wang, X. Song, X. Li, B. Liu, Z. Xiong and B. Lai, *Environ. Sci. Technol.*, 2023, **57**, 14071–14081.
136 Y. Huang, W. Huang, L. Dou, L. Li, C. Liu, B. Lai and N. Li, *J. Cleaner Prod.*, 2025, **493**, 144934.
137 L. Ge, J. Wei, J. He, R. Sun, W. Wang, D. Yang, J. Lu, P. Hong, Y. Li, Y. Li, C. Xie, Z. Wu and L. Kong, *Chem. Eng. J.*, 2025, **512**, 162104.
138 M. Gao, Y. Ren, W. Zheng, M. Liu, X. Wang, N. Nanayakkara and Y. Liu, *Appl. Catal., B*, 2025, **371**, 125218.
139 F. Xu, C. Lai, M. Zhang, B. Wang, B. Li, D. Ma, X. Zhou, L. Li, H. Yan, X. Huo, S. Liu, Y. Fu and L. Tang, *J. Colloid Interface Sci.*, 2025, **688**, 421–431.
140 C. Zhu, F. Cun, Y. Nie, Q. Du, F. Lao, C. Yue, F. Liu and A. Li, *Appl. Catal., B*, 2024, **358**, 124409.
141 Q.-Y. Wu, Z.-W. Yang, Z.-W. Wang and W.-L. Wang, *Proc. Natl. Acad. Sci. U. S. A.*, 2023, **120**, e2219923120.
142 J. Zheng, Q. Lin, Y. Wu, Y. Liu, C. Zeng, Y. Luo and T. Chen, *Chem. Eng. J.*, 2024, **489**, 151307.
143 X. Liu, D. Huang, C. Lai, L. Qin, S. Liu, M. Zhang and Y. Fu, *J. Colloid Interface Sci.*, 2023, **629**, 417–427.
144 X.-C. Feng, Z.-J. Xiao, H.-T. Shi, B.-Q. Zhou, Y.-M. Wang, H.-Z. Chi, X.-H. Kou and N.-Q. Ren, *Environ. Sci. Technol.*, 2022, **56**, 14048–14058.
145 X. Fu, Q. Zeng, L. Song, Y. Wu, R. Wang and Q. Zeng, *Chem. Eng. J.*, 2024, **497**, 154668.
146 X. Fu, Q. Zeng, Y. Gao, L. Song, Y. Wen, T. Cai, Q. Zhang, C. Hu and Q. Zeng, *ACS ES&T Eng.*, 2024, **4**, 903–914.
147 W. Du, Q. Zhang, Y. Shang, W. Wang, Q. Li, Q. Yue, B. Gao and X. Xu, *Appl. Catal., B*, 2020, **262**, 118302.
148 Y. Li, J. Hu, Y. Zou, L. Lin, H. Liang, H. Lei, B. Li and X.-y. Li, *Chem. Eng. J.*, 2023, **453**, 139890.
149 Y. Chai, H. Dai, X. Duan, Z. Sun, F. Hu, J. Qian and X. Peng, *Appl. Catal., B*, 2024, **341**, 123289.
150 Y. Zou, J. Hu, B. Li, L. Lin, Y. Li, F. Liu and X.-y. Li, *Appl. Catal., B*, 2022, **312**, 121408.
151 H. Dai, Z. Zhao, K. Wang, F. Meng, D. Lin, W. Zhou, D. Chen, M. Zhang and D. Yang, *J. Hazard. Mater.*, 2024, **465**, 133399.
152 X. Zhao, X. Jia, H. Li, H. Zhang, X. Zhou, Y. Zhou, H. Wang, L. Yin, T. Wågberg and G. Hu, *Chem. Eng. J.*, 2022, **450**, 138098.
153 J. Song, N. Hou, X. Liu, M. Antonietti, P. Zhang, R. Ding, L. Song, Y. Wang and Y. Mu, *Adv. Mater.*, 2023, **35**, 2209552.
154 Y. Jiang, Y. Tan, M. Sun, W. Jiang, S. Zhou, B. Liu and C. Liu, *J. Environ. Chem. Eng.*, 2025, **13**, 115229.
155 T. He, Y. Lu, S. Han, J. Hu, P. Gao, F. Xiao and S. Yang, *J. Catal.*, 2025, **442**, 115920.
156 Y. Ma, X. Liu, M. Tang, K. Du, H. Yin, X. Mao and D. Wang, *Chem. Eng. J.*, 2022, **440**, 135879.
157 B. Li, Z. Wang, L. Sun, J. Wu, L. Liu, J. Liu, S. Liu, S. Chen, T. Wang, P. Wu, N. Zhu and Z. Dang, *Appl. Catal., B*, 2025, **372**, 125280.
158 Q. Shi, W. Zhu, W. Wang, F. Xie and Y. Feng, *Chem. Eng. J.*, 2025, **517**, 164407.
159 L. K. Chen, K. W. Xing, Q. K. Shentu, Y. F. Huang, W. Y. Lv and Y. Y. Yao, *Chemosphere*, 2021, **280**, 130911.
160 W. Li, H. Zeng, Z. Zhou, L. Li, R. Tang, C. Ding, D. Gong and Y. Deng, *Chem. Eng. J.*, 2025, **520**, 166214.
161 M. T. Zhang, H. Li, J. X. Chen, F. X. Ma, L. Zhen, Z. H. Wen and C. Y. Xu, *Adv. Funct. Mater.*, 2023, **33**, 2209726.
162 H. Li, N. Wang, H. Li, Z. Ren, W. Ma, J. Li, Y. Du and Q. Xu, *Appl. Catal., B*, 2024, **341**, 123323.
163 Y. Zhang, X. Chen, C. Liang, L. Yin and Y. Yang, *Appl. Catal., B*, 2022, **315**, 121536.
164 K. Zhu, W. Qin, Y. Chen, X. Liang, H. Xin, Z. Huang, H. F. Garces, Y. Gan, M. Sillanpää, R. Qiu, G. Guan and K. Yan, *Nano Today*, 2024, **58**, 102462.
165 M. Wang, R. Jiang, G. Lu, T. Dang, Y. Chen, J. Liu and J. Hou, *Chem. Eng. J.*, 2025, **507**, 160546.
166 C. Zhu, Y. Nie, F. Cun, Y. Wang, Z. Tian and F. Liu, *Appl. Catal., B*, 2022, **319**, 121900.
167 J. Qin, Q. Wang, B. Han, C. Jin, C. Luo, Y. Sun, Z. Dai, S. Wang, H. Liu, X. Zheng and Z. Hu, *Appl. Catal., B*, 2025, **360**, 124538.
168 H. Zhao, Y. Liu, D. Wu, H. Yu, X. Zhang, H. Wang, X. Shang and M. Lv, *Environ. Pollut.*, 2023, **335**, 122298.
169 M. Yang, H. Li, F. Liu, S. Sun, J. Mei, Y. Jiao, J. Cui, Y. Xu, H. Song, Z. Duan, W. Liu and Y. Ren, *Appl. Catal., B*, 2024, **354**, 124071.
170 H. Xia, W. Yang, H. Xu, C. Ye, M. Liang, B. Cui, C. Zou, Y. Zeng, Y. Qu and F. Lu, *Sep. Purif. Technol.*, 2024, **330**, 125273.

171 Y. Q. Liu, L. Tian, M. Huang, H. Z. Liu, Z. Y. Guo, J. Ding, W. Q. Xia, L. Teng, H. Q. Yu and W. W. Li, *Environ. Sci. Technol.*, 2025, **59**, 880–891.
172 H. J. Khan, J. Ding, J. Qu, G. V. Sarrigani, P. Fitzgerald, X. Xu, A. E. Ghadi, Q. Sui, C. Tian, J. M. Cairney, D. Wiley and D. Wang, *Appl. Catal., A*, 2025, **706**, 120469.
173 A. Han, B. Wang, A. Kumar, Y. Qin, J. Jin, X. Wang, C. Yang, B. Dong, Y. Jia and J. Liu, *Small Methods*, 2019, **3**, 1800471.
174 W. Yang, P. Hong, D. Yang, Y. Yang, Z. Wu, C. Xie, J. He, K. Zhang, L. Kong and J. Liu, *J. Colloid Interface Sci.*, 2021, **597**, 56–65.
175 L. Pang, S. Wang, X. Jia, Y. Wang, J. Li and H. Liu, *J. Alloys Compd.*, 2024, **972**, 172856.
176 P. Garg, M. Chauhan, P. Attri, B. Kumari, G. Kaur and G. R. Chaudhary, *ACS Appl. Mater. Interfaces*, 2025, **17**, 23911–23922.
177 H. Li and J. Liu, *Curr. Opin. Chem. Eng.*, 2023, **41**, 100940.
178 W. Kong, Z. Liu, J. Wu, C. Wen, J. Yan, Y. Gao, G. Li, X. Wang and M. Huo, *Process Saf. Environ.*, 2025, **195**, 106778.
179 S. Zhou, Y. Yang, R. Wang, Y. Cui, S. Ji, L. Du and F. Jiang, *J. Colloid Interface Sci.*, 2025, **680**, 307–325.
180 S. Zhou, R. Wang, Y. Yang, A. Xiao, X. Pan and F. Jiang, *Chem. Eng. J.*, 2025, **513**, 163031.
181 Q. Peng, G. Wen, C. Yuan, C. Lv, L. Wu, J. He and X. Hou, *J. Mater. Chem. A*, 2024, **12**, 29033–29043.
182 C. Zhu, M. Yang, B. Jiang, L. Lu, Q. Fang, Y. Zheng, S. Song, B. Chen and Y. Shen, *Nat. Commun.*, 2025, **16**, 790.
183 Z. Q. Zhang, P. J. Duan, J. X. Zheng, Y. Q. Xie, C. W. Bai, Y. J. Sun, X. J. Chen, F. Chen and H. Q. Yu, *Nat. Commun.*, 2025, **16**, 115.
184 S. Liu, J. Du, H. Wang, W. Jia, Y. Wu, P. Qi, S. Zhan, Q. Wu, J. Ma, N. Ren and W. Q. Guo, *Water Res.*, 2024, **254**, 121417.
185 W. Fu, Z. Liu, D. Li and B. Pan, *Water Res.*, 2025, **275**, 123173.
186 C. Bie, J. Yang, X. Zeng, Z. Wang, X. Sun, Z. Yang, J. Yu and X. Zhang, *Small*, 2025, **21**, e2411184.
187 T. Zeng, X. Tang, Z. Huang, H. Chen, S. Jin, F. Dong, J. He, S. Song and H. Zhang, *Environ. Sci. Technol.*, 2023, **57**, 20929–20940.
188 H. Zhao, J. Peng, Z. Chen, Y. Zhou, M. Xu, H. Zhang and X. Zhao, *Chem. Eng. J.*, 2024, **497**, 154831.
189 X. Zhao, X. Li, Z. Zhu, W. Hu, H. Zhang, J. Xu, X. Hu, Y. Zhou, M. Xu, H. Zhang and G. Hu, *Appl. Catal., B*, 2022, **300**, 120759.
190 B. Huang, Z. Wu, X. Wang, X. Song, H. Zhou, H. Zhang, P. Zhou, W. Liu, Z. Xiong and B. Lai, *Environ. Sci. Technol.*, 2023, **57**, 15667–15679.
191 S. Iijima, *Nature*, 1991, **354**, 56–58.
192 L. Yang, G. Sun, H. Fu and L. Zhang, *Chem. Eng. J.*, 2023, **472**, 145052.
193 H. Zhao, K. Yin, Q. Yue, W. Yin, B. Gao and Y. Gao, *J. Hazard. Mater.*, 2025, **491**, 137971.
194 K. Yin, Y. Tang, Z. Li, H. Zhao, X. Xu, Q. Li, Q. Yue, Y. Gao and B. Gao, *Water Res.*, 2025, **285**, 124130.
195 J. Jiang, S. Liu, B. Zhao, T. Sun, Y. Zhang, R. Wang, M. Huo, D. Zhou, C. Zhou and S. Dong, *Adv. Mater.*, 2025, **37**, e2417834.
196 C. Chen, M. Yan, Y. Li, Y. Hu, J. Chen, S. Wang, X. Wu and X. Duan, *Appl. Catal., B*, 2024, **340**, 123218.
197 Y. Meng, Y. Liu, C. Wang, Y. Si, Y. Wang, W. Xia, T. Liu, X. Cao, Z. Guo, J. Chen and W. Li, *Nat. Commun.*, 2024, **15**, 5314.
198 Y. Pan, X. Wang, W. Zhang, L. Tang, Z. Mu, C. Liu, B. Tian, M. Fei, Y. Sun, H. Su, L. Gao, P. Wang, X. Duan, J. Ma and M. Ding, *Nat. Commun.*, 2022, **13**, 3063.
199 X. You, Z. Guo, Q. Jiang, J. Xia, S. Wang, X. Yang, Z. Zhuang, Y. Li, H. Xiang, H. Li and B. Yu, *Nano Lett.*, 2025, **25**, 8704–8712.